Chapter 1
Introduction: Low-Temperature Fuel Cells

T. W. Napporn, A. Mokrini, and F. J. Rodríguez-Varela

Abstract This chapter describes the reactions occurring in low-temperature fuel cells, fuelled with from the most common H_2, to several organic molecules. The differences in the complexity of the anode reactions and their effect on the energy that may be generated from the fuel cells are discussed. It is established that, even though H_2/O_2 fuel cells are the most performing in terms of power density for large-demand systems, the use of liquid fuels is advantageous for several low-power applications. The performance of nanostructured anode and cathode catalysts in complete fuel cell systems is also covered. It is indicated that in alkaline media, some non-Pt nanocatalysts have a high catalytic activity, particularly for the ORR. Even more, the recent advances in polymer electrolyte membranes are shown, from the widely used commercial Nafion®, to the more recently developed anionic polymers for anion exchange membrane fuel cells. It is concluded that compatibility of composite and blend materials with the host ionomer is critical for the development of stable low-temperature fuel cells.

Keywords Proton exchange membrane fuel cells (PEMFC) · Anion exchange membrane fuel cells (AEMFC) · Perfluorosulfonic-acid membranes (PFSA) · Direct methanol AEMFCs (DM-AEMFCs) · Direct ethanol AEMFCs (DE-AEMFCs) · Direct ethylene Glycol AEMFCs (DEG-AEMFCs) · Direct glycerol AEMFCs (DG-AEMFCs) · Non-platinum group metal (PGM) · Perfluorinated PEMs · Nafion® membranes · Partially fluorinated PEMs · Hydrocarbon PEMs · Anion exchange

T. W. Napporn
Université de Poitiers, IC2MP UMR-CNRS 7285, Poitiers Cedex 9, France

A. Mokrini
NRC Automotive and Surface Transportation Research Center, Boucherville, QC, Canada

F. J. Rodríguez-Varela (✉)
Sustentabilidad de los Recursos Naturales y Energía, Cinvestav Unidad Saltillo, Ramos Arizpe, Mexico
e-mail: javier.varela@cinvestav.edu.mx

© Springer International Publishing AG, part of Springer Nature 2018

F. J. Rodríguez-Varela, T. W. Napporn (eds.), *Advanced Electrocatalysts for Low-Temperature Fuel Cells*, https://doi.org/10.1007/978-3-319-99019-4_1

membranes (AEMs) · Hydrogen oxidation reaction (HOR) · Tafel reaction · Heyrovsky reaction · Volmer reaction · Oxygen reduction reaction (ORR) · Rotating ring disk electrode (RRDE) · Koutecky–Levich plots

1.1 Introduction

Proton exchange membrane and anion exchange membrane fuel cells (PEMFC and AEMFC, respectively) have gained the attention of academic and industrial research groups, due to their capacity to generate high-power density at low temperatures. Ever since the advancements in the 1960s for space industry applications, both systems have experienced to an extent a technological development to reach near-commercialization status. This is particularly the case of PEMFCs, whose performance has been greatly improved by the use of the perfluorosulfonic acid membranes and the demonstration of high interfacial area gas diffusion electrodes at Los Alamos National Laboratories [1, 2]. The new electrode structure proposed in those studies has reduced the catalyst loading (i.e., Pt) by an order of magnitude [1]. PEMFC is a more advanced technology than AEMFC. However, fuel cells using anion exchange membrane are being studied with a significant interest in recent years due to the development of chemically stable alkaline polymers and the capability of using non-noble metals to catalyze the electrochemical reactions in basic media. The following sections introduce the electrochemical reactions taking place in AEMFCs working with hydrogen and liquid fuels. Also, the performance of several nanostructured electrocatalysts in complete fuel cell systems is shown. Moreover, the latest developments in membranes for PEM and AEM fuel cells are discussed.

1.2 Electrocatalytic Reactions in Anion Exchange Membrane Fuel Cells (AEMFCs)

In first half of the twentieth century, the research in alkaline fuel cells (AFCs) led this type of cell to be considered for several applications. Francis T. Bacon worked in the development of H_2/O_2 AFCs, which resulted in demonstrative programs of capacity up to 5 kW output [1–3]. AFC systems reached a status that allowed the technology to be considered for space applications [1]. However, disadvantages of AFCs included several restrictions, among them, the need to use fuels and oxidants free of CO_2 due to the risk of carbonation with KOH and NaOH [1, 4]. Also, the management of liquid-phase electrolytes has been a relevant issue in AFCs [5]. With the development of the polymer electrolyte membrane fuel cells (PEMFCs) based on Nafion®, the research on AFCs somehow decreased, particularly in the 1990s and early twenty-first century.

Over the past decade, however, AEMFCs have received increased attention of fuel cells science and technology research laboratories [6]. First of all, it is generally acknowledged that the kinetics of the electrochemical cathode reactions in alkaline media is faster compared to their acid counterpart (i.e., PEMFCs). Also, perhaps one the most attracting characteristics of AEMFCs is the possibility of using non-PGM (Pt group metals) or non-noble metal catalysts in anodes and cathodes to promote the hydrogen oxidation reaction (HOR) and the oxygen reduction reaction (ORR) [6–9]. Even more, regardless of its relatively low operation temperature, AEMFCs can also operate with liquid fuels as an alternative to hydrogen [10–14].

In fact, it has been reported that AEMFCs can operate with a CH_4 containing 5% H_2 [15]. In spite of the capability of using different fuels, attention must be paid to the purity of the oxidant, since as mentioned CO_2-containing air leads to carbonation by reacting with OH^- anions. The report by Dekel et al. indicates that bicarbonate (HCO_3^-) and carbonate (CO_3^{2-}) anions are formed, changing the anion composition of the anion exchange membrane [16]. Thus, the use of air as oxidant which may contain CO_2 decreases the cell performance [16, 17].

Nevertheless, the promoted attraction offered recently by AEMFCs can be attributed to the important advances in high-performance anion exchange membranes, even though one relevant issue is the ionomer stability [6, 18–20]. As pointed out by Varcoe et al., the first publication of the so-called alkaline membrane fuel cells (AMFCs) appeared in 2005 [18]. Ever since, the number of publications has clearly increased. Dekel has reported that the number of reports has overpassed 2000 in the 2013–2017 period (Fig. 1.1) [6]. Evidently, advances in the different components of AEMFCs other than membranes, including high performance and durable catalysts, will impulse the research and applications of this technology to new grounds.

In the following sections, the electrocatalytic reactions in AEMFCs fuelled with different fuels are given. The selection of fuels goes from H_2, to several of the most common C-containing fuels: methanol (CH_3OH), ethanol (C_2H_5OH), ethylene glycol ($C_2H_6O_2$), and glycerol ($C_3H_8O_3$). Each of the liquid fuels introduces cost and energetic advantages and disadvantages. But perhaps it is worth analyzing their use from a sustainability point of view, and therefore the feasibility of obtaining them from biomass resources.

1.2.1 H_2/O_2 AEMFCs

In terms of power density and catalyst durability, the most performing AEMFC is the H_2/O_2 cell. A power density of 1.4 W cm^{-2} has been reported by Varcoe et al., with the cell operating at 60 °C, equipped with an AEM based on radiation-grafted ethylene tetrafluoroethylene and PtRu/C (anode) and Pt/C (cathode) catalysts [21]. The same research group has reported the performance of an H_2/O_2 AEMFC with non-PGM cathode catalysts (1.0 mg_{Ag} cm^{-2}) having a power density above 1 W cm^{-2} [22]. The stability of H_2/O_2 AEMFCs has also been evaluated. Yu et al.

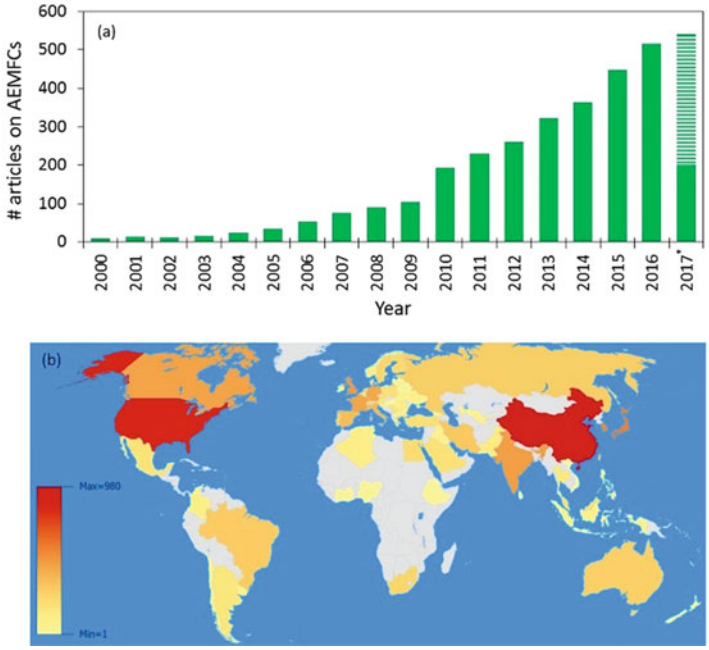

Fig. 1.1 (**a**) Reports published in the 2013–2017 period covering research on AEMFCs, (**b**) distribution by country of origin (reproduced from Ref. [6] with kind permission of © Elsevier)

have tested a cell for 500 h, with a decrease in cell voltage of 0.22 mV h^{-1}. The cell used quaternary ammonium SEBS as the ionomer [23].

In H_2/O_2 AEMFCs the electrochemical anode and cathode half-cell reactions, as well as the overall cell reaction, with their corresponding potentials at standard conditions are:

Anode reaction:

$$2H_2 + 4OH^- \rightarrow 4H_2O + 4e^-, E_a^o = 0.83 \text{ V vs.SHE} \tag{1.1}$$

Cathode reaction:

$$O_2 + 2H_2O + 4e^- \rightarrow 4OH^-, E_c^o = 0.40 \text{ V vs.SHE} \tag{1.2}$$

Overall:

$$2H_2 + O_2 \rightarrow 2H_2O, E_{\text{cell}} = 1.23 \text{ V} \tag{1.3}$$

H_2/O_2 AEMFCs are attractive from an economical point of view because of the feasibility of using non-PGM catalysts for the ORR and for the HOR [24]. However,

it should be mentioned that high performances have been reported when using catalysts such as Ir or Pd to promote the HOR either in half-cell experiments or in full AEMFC tests [25, 26].

1.2.2 Direct Methanol AEMFCs (DM-AEMFCs)

The enhanced kinetics of the methanol oxidation reaction (MOR) in 0.5 mol/l K_2CO_3 and 1 mol/l $KHCO_3$ electrolytes compared with a 0.5 mol/l H_2SO_4 solution, foreseen the use of CH_3OH in AEMFCs, has been discussed by Zhuang et al. [27]. By performing in-situ FTIR analysis, the authors concluded that methanol could be oxidized to CO_2 in those alkaline solutions. Scott and Hao have evaluated extensively a direct methanol alkaline fuel cell using Pt/C anode and cathode catalyst. The cell performance increased at higher temperatures (up to 60 °C). On the other hand, with the anion exchange membranes used, the crossover of methanol to the anode increased at higher fuel concentrations [28]. Kim et al. have reported the same effect in an air-breathing direct methanol fuel cell with anion exchange membrane when increasing the CH_3OH concentration from 7 to 10 M [29]. Even though it has been reported that AEMFCs fuelled with methanol are less performing compared to other liquid fuels [30], Bianchini et al. reported an enhanced performance of a direct methanol AEMFC at 60 °C with a Pd/MWCNT anode, compared to ethanol and glycerol [31].

In DM-AEMFCs the electrochemical reactions are:

Anode reaction:

$$CH_3OH + 6OH^- \rightarrow CO_2 + 5H_2O + 6e^-, E_a^o = -0.81 \text{ V vs.SHE} \quad (1.4)$$

Cathode reaction:

$$3/2O_2 + 3H_2O + 6e^- \rightarrow 6OH^-, E_c^o = 0.40 \text{ V vs.SHE} \quad (1.5)$$

Overall:

$$CH_3OH + 3/2O_2 \rightarrow CO_2 + 2H_2O, E_{\text{cell}} = 1.21 \text{ V} \quad (1.6)$$

1.2.3 Direct Ethanol AEMFCs (DE-AEMFCs)

The use of ethanol in fuel cells is of interest, since this organic molecule is considered a carbon neutral and sustainable fuel [32]. Even more, bioethanol from biomass has been used as the fuel in DE-AEMFCs, where a power density of ca. 90 mW cm^{-2} has been generated using a dealloyed PtCo/CNT anode

catalyst [33]. A power density of around 50 mW cm^{-2} has been obtained elsewhere using Pd-based catalysts at the anode fuelled with 1.0 mol L^{-1} ethanol +0.5 mol L^{-1} NaOH [34]. In their study, Fujiwara et al. have compared the performance of DEFCs equipped with anion and cation exchange membranes [35]. The power density generated with the AEM was about ten times higher, compared to the cationic counterpart. Nevertheless, due to the low OH^- conductivity of the membrane, 0.5 mol L^{-1} KOH had to be provided along with the 1.0 mol L^{-1} ethanol fuel at the anode in order to sustain a high performance. Recently, a passive DE-AEMFC stack delivering a peak power density of 38 mW cm^{-2} at room temperature, using PdNi/C anode catalysts and $FeCuN_4$/C cathode catalysts, has been demonstrated by Zhao and Li [36].

The electrochemical reactions in DE-AEMFCs are:

Anode reaction:

$$C_2H_5OH + 12OH^- \rightarrow 2CO_2 + 9H_2O + 12e^-, E_a^o = -0.74 \text{ V vs.SHE} \quad (1.7)$$

Cathode reaction:

$$3O_2 + 6H_2O + 12e^- \rightarrow 12OH^-, E_c^o = 0.40 \text{ V vs.SHE} \quad (1.8)$$

Overall:

$$C_2H_5OH + 3O_2 \rightarrow 2CO_2 + 3H_2O, E_{cell} = 1.14 \text{ V} \quad (1.9)$$

1.2.4 Direct Ethylene Glycol AEMFCs (DEG-AEMFCs)

Ethylene glycol (EG) has been used in fuel cells as a feasible alternative to replace methanol and ethanol. For this application, $C_2H_6O_2$ is safer to handle than methanol, is less toxic than methanol and ethanol, and its electron transfer rate is higher during oxidation than ethanol [37–39]. EG can also be produced from biomass and its partial selective oxidation in a DEG-AEMFC can generate valuable oxalic acid without CO_2 emissions [40]. The power density generated from a DEG-AEMFC at 60 °C has been shown to become higher by increasing the fuel concentration from 0.5 to 1.0, but decreases with 2 mol L^{-1} $C_2H_6O_2$ (with a KOH concentration of 1 mol L^{-1}) [39]. Such cell used an alkali-doped PBI membrane. Cremers et al. have compared the performance of DEG-AEMFCs equipped with KOH-doped PBI and a quaternary amine alkaline AEM, with the later generating a higher power density [41]. KOH-doped Nafion ® has also been used by Forbicini et al. in a DEG-AEMFC [42]. Evidently, DEG-AEMFCs equipped with several formulations of AEMs have been tested [43, 44]. It has been reported that the power density generated by

DEG-AEMFCs is higher than those of fuel cells fuelled with methanol, ethanol, and 1,2-propanediol, but slightly lower than in the case of glycerol [10, 44–46].

The electrochemical reactions in DEG-AEMFCs are:

Anode reaction:

$$C_2H_6O_2 + 10OH^- \rightarrow 2CO_2 + 8H_2O + 10e^-, E_a^o = -0.81 \text{ V vs.SHE} \quad (1.10)$$

Alternatively, the partial oxidation of EG to oxalate is [44]:

$$C_2H_6O_2 + 10OH^- \rightarrow (COO^-)_2 + 8H_2O + 8e^-, E_a^o = -0.81 \text{ V vs.SHE} \quad (1.11)$$

Cathode reaction:

$$5/2O_2 + 5H_2O + 10e^- \rightarrow 10OH^-, E_c^o = 0.40 \text{ V vs.SHE} \quad (1.12)$$

Overall:

$$C_2H_6O_2 + 5/2O_2 \rightarrow 2CO_2 + 3H_2O, E_{\text{cell}} = 1.21 \text{ V} \quad (1.13)$$

1.2.5 Direct Glycerol AEMFCs (DG-AEMFCs)

Glycerol has several advantages for fuel cell applications: it has a relatively low toxicity, high energy density, its crossover rate is low, and is relatively inexpensive [47, 48]. It is also a versatile fuel, since DG-AEMFCs have been operated as co-generators of electricity and valuable chemicals [49, 50]. Pt and Pd-based catalysts are normally used as anode catalysts in DG-AEMFCs [47, 48, 51–54]. However, Au-based nanomaterials have also shown a high catalytic activity for the oxidation of the molecule [49, 50, 55]. Li et al. have demonstrated a higher power density generated by a DG-AEMFC in the 50–80 °C temperature range with an Au/C anode (1.0 mol L^{-1} glycerol +2.0 mol L^{-1} KOH, Fe-Cu-N_4/C cathode), compared to a PEM DGFC at 90 °C (1.0 mol L^{-1} glycerol, PtRu/C anode, Pt/C cathode) [55]. It has been shown also that higher power density is generated from the DG-AEMFC, relative to DM and DEG-AEMFCs, with the same fuel concentration [55].

One more advantage of glycerol is that it can be used in its crude composition as obtained from the bio-diesel manufacturing industry, as reported by Li′s group [51, 54–56]. Crude glycerol is cheaper than refined glycerol, methanol, and ethanol [56]. Using 1.0 mol L^{-1} crude glycerol (+ 2.0 mol L^{-1} KOH), a DG-AEMFC generated a power density of ca. 40 mW cm^2 (anode: Au/C; cathode: Fe-Cu-N_4/C; AEM: A201, 28 mm, Tokuyama, 80 °C) [55].

The electrochemical reactions in DG-AEMFCs are shown below. According to some workers, the oxidation of glycerol in alkaline media may proceed through the formation of glycerate or tartronic acid [57, 58]. Following the tartronic acid route:

Anode reaction [58]:

$$C_3H_8O_3 + 8OH^- \rightarrow C_3H_4O_5 + 6H_2O + 8e^-, E_a^o = -0.77 \text{ V vs.SHE} \quad (1.14)$$

$$C_3H_4O_5 + 2OH^- \rightarrow (C_3H_2O_5)^{2-} + 2H_2O \quad (1.15)$$

Cathode reaction:

$$2O_2 + 4H_2O + 8e^- \rightarrow 8OH^-, E_c^o = 0.40 \text{ V vs.SHE} \quad (1.16)$$

Overall:

$$C_3H_8O_3 + 2O_2 + 2OH^- \rightarrow (C_3H_2O_5)^{2-} + 4H_2O, E_{cell} = 1.17 \text{ V} \quad (1.17)$$

1.2.6 AEMFCs Operating with Other Fuels

Other fuels have been evaluated at AEMFCs. For example, the reactions at direct borohydride (DB, Eqs. 1.18, 1.19, and 1.20) and direct formate (DF, Eqs. 1.21, 1.22, and 1.23) AEMFCs are [13, 59]:

For DB-AEMFCs:

Anode reaction:

$$BH_4^- + 8OH^- \rightarrow BO_2^- + 6H_2O + 8e^-, E_a^o = -1.24 \text{ V vs.SHE} \quad (1.18)$$

Cathode reaction:

$$O_2 + 2H_2O + 4e^- \rightarrow 4OH^-, E_c^o = 0.40 \text{ V vs.SHE} \quad (1.19)$$

Overall:

$$BH_4^- + 2O_2 \rightarrow BO_2^- + 2H_2O, E_{cell} = 1.64 \text{ V} \quad (1.20)$$

and

For DF-AEMFCs:

Anode reaction:

$$HCOO^- + 3OH^- \rightarrow CO_3^{2-} + 2H_2O + 2e^-, E_a^o = -1.05 \text{ V vs.SHE} \quad (1.21)$$

Cathode reaction:

$$1/2O_2 + H_2O + 2e^- \rightarrow 2OH^-, E_c^o = 0.40 \text{ V vs.SHE} \quad (1.22)$$

Overall:

$$HCOO^- + 1/2O_2 + OH^- \rightarrow CO_3^{2-} + 2H_2O, E_{cell} = 1.45 \text{ V} \quad (1.23)$$

Additionally, Ogumi et al. compared the performance of fuel cells fed with the polyalcohols, erythritol and xylitol, with those of ethylene glycol, glycerol, and methanol. It has been concluded that the higher power density is delivered by using ethylene glycol with the AEMFC operating at 323 K, with a Pt-Ru/C anode and Pt/C cathode [30].

1.3 Performance of Several Types of Nanostructured Anodes and Cathodes in AEMFCs

As discussed in Sect. 1.1, several fuels are being used in AEMFCs, from H_2 to organic molecules. Advantages and disadvantages of each of them seem to be clear. Higher power densities can be delivered by H_2/O_2 AEMFCs due to the high reactivity of the gaseous fuel. Also, the absence of C atoms avoids the need of C–C bonds cleavage and the formation of reaction intermediates such as CO_{ads} during the HOR. However, hydrogen is not freely available in nature and must be produced, mainly from hydrocarbons. Renewable hydrogen, i.e., from water electrolysis using solar or wind resources, is feasible, but still more expensive than natural gas reforming on a large-scale basis.

On the other hand, easier handling of the fuels compared to H_2 can be achieved with liquid molecules. Very important from a sustainability point of view, some of the organic fuels can be produced from biomass resources. Nevertheless, the power density obtained from AEMFCs is lower when fuelled with such liquid molecules relative to hydrogen [6]. Moreover, the operational problems caused by the cross-over phenomena remain in AEMFCs (to a less extent than in PEMFCs) using methanol, ethanol, or other liquid fuels. Therefore, the selection of nanostructured cathode catalysts is of high relevance to avoid depolarization losses caused by crossed fuel or reaction intermediates. As mentioned earlier, the kinetics of the ORR in alkaline media is faster than in acid electrolytes, allowing for the use of a number of high-performance cathodes, from Pt/C and Pd/C (and their alloys or composite materials with metal oxides), to non-PGM and metal-free nanocatalysts. Taking advantage of this variety that includes low-cost nanomaterials, AEMFCs may be a cheaper technology than PEMFCs.

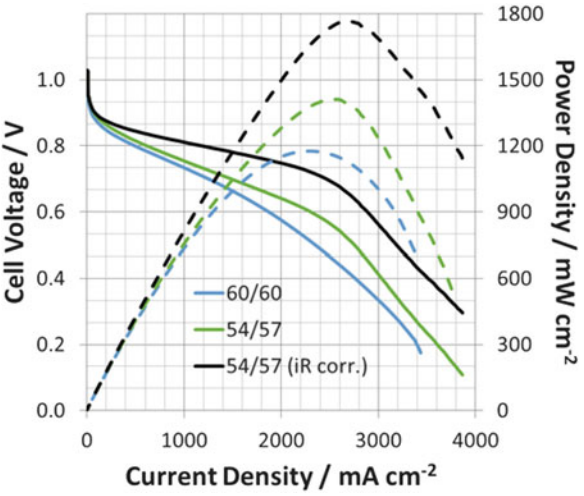

Fig. 1.2 Polarization curves of H_2/O_2 AEMFCs. Experimental conditions with 54/57 anode/cathode dew points: anode: 0.67 mg_{PtRu} cm^{-2} on 5% PTFE, cathode: 0.53 mg_{Pt} cm^{-2} on 5% PTFE GDL. Cell temperature: 60 °C (adapted from Ref. [21], reproduced with kind permission of © Elsevier)

Recent reports show the performance of AEMFCs under different operating conditions. Using a 0.53 mg_{Pt} cm^{-2} Pt/C cathode (40 wt. %), a power density of 1.4 W cm^{-2} has been delivered by a H_2/O_2 AEMFC operating at 60 °C (with an ETFE-g-VBCTMA membrane) as seen in Fig. 1.2 [21]. Power densities of 1.16 and 0.91 W cm^{-2} have been obtained from H_2/O_2 AEMFCs operating at 60 °C, with Pt/C cathodes, PtRu/C anodes, and RG-AEM(Cl^-) membranes [60]. The same group has reported a H_2/O_2 AEMFC delivering power densities of 1.1 and 0.699 W cm^{-2} using a non-Pt cathode (Ag/C, 1.0 mg_{Ag} cm^{-2}), operating with O_2 and CO_2-free air, respectively [22]. It has been reported by the authors that the Ag/C outperformed a Pt/C cathode with CO_2-free air at the cathode. Elsewhere, a peak power density of 1.0 W cm^{-2} has been reported with a H_2/O_2 AEMFC equipped with commercial Pt/C cathode and PtRu/C anode (metal loadings of 0.4 mg cm^{-2}) membrane of the aQAPS-Sx type and $T_{cell} = 60$ °C [61]. Also, a Pt-free H_2 (dry)/Air (<10 ppm CO_2) AEMFC operating at 73 °C delivered a power density of 0.5 W cm^{-2} (cathode: Ag, 3.0 mg_{Ag} cm^{-2}; anode: Pd/C-CeO_2) [26]. Moreover, a H_2 (dry)/Air (CO_2 free) AEMFC with a silver-based alloy (3.0 mg cm^{-2}) cathode and a Pd/Ni anode generated 0.4 W cm^{-2} power density at 73 °C [62].

It is therefore feasible to use non-Pt cathode catalysts and yet generate high-power densities not only from H_2/O_2 AEMFCs, but also from fuel cells using liquid fuels. Mesoporous Fe/N/C cathode catalysts with highly active Fe-Nx/C sites have been used in a H_2/O_2 AEMFC (A901 membrane, Tokuyama), exhibiting 40% higher power density (0.272 W cm^{-2}) than commercial Pt/C in single-cell tests with $T_{cell} = 50$ °C. The high performance of the non-Pt catalyst has been in part attributed to large pores in the mesoporous structure, which resulted in a high surface area and accessibility to the active sites [63]. Elsewhere, a H_2/O_2 AEMFC (membrane Tokuyama A201) containing a Fe-NMG (a type of Fe-N-C) cathode catalyst and Pt/C anode generated 0.218 W cm^{-2}, a higher value than 0.2 W cm^{-2} of a cell with Pt/C cathode and anode catalysts with $T_{cell} = 70$ °C (Fig. 1.3) [7]. A H_2/O_2 AEMFC

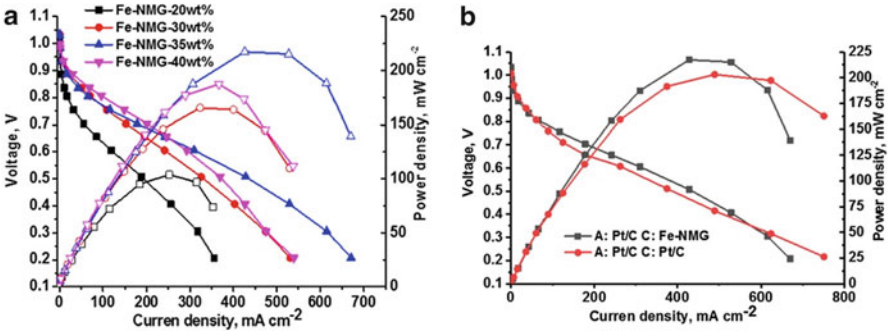

Fig. 1.3 Polarization curves of AEMFCs with (**a**) Fe-NMG cathodes at different ionomer concentration, (**b**) comparison of the performance of MEAs having Fe-NMG cathode and Pt/C anode catalysts, and Pt/C catalysts on both anode and cathode (reproduced from Ref. [7] with kind permission of © Elsevier)

composed of CoPPY/C-based cathodes and Ni-W-based anodes produced 0.04 W cm^{-2} at 60 °C, with a membrane of the xQAPS type [64].

Other types of AEMFCs have also reached a good development. It has been reported that a DM-AEMFC may produce 0.046 W cm^{-2} at 60 °C with Fe_2O_3/Mn_2O_3 (3:1) cathode and PtRu/C anode, and a polymer fiber membrane [65]. Elsewhere, a DM-AEMFC with MnO_2 cathode catalyst (membrane: Q-PVA/PECH; anode: PtRu/C) generates a maximum power density of 0.022 W cm^{-2} at 25 °C [66]. Using a similar cathode composition and a PVA/HAP membrane, an air-breathing DM-AEMFC has generated 0.011 W cm^{-2} at 25 °C (Ti-based anode with PtRu black) [67]. Recently, mesoporous 3D nitrogen-doped yolk-shelled carbon spheres have been used as cathodes in a DM-AEMFC, delivering 0.056 and 0.141 W cm^{-2} at 25 and 60 °C, respectively (polymer fiber membranes; PtRu anodes) [68].

Non-noble Fe-N-C catalyst has also been used in a DE-AEMFC, reaching a power density of 0.062 W cm^{-2} with 50 wt. % Nafion® content, Pt-Ru/C anode, and KOH-doped PBI membrane (T_{cell} = 90 °C) [8]. A higher power density (0.335 W cm^{-2}) has been generated by a DE-AEMFC equipped with a Fe-Co/C cathode, anode of the combined Pd/TNTA-web type, T_{cell} = 80 °C, and Tokuyama A201 membrane [45]. With these components, ethanol as the fuel outperformed the use of glycerol and ethylene glycol. Other fuels have been evaluated. For example, a DEG-AEMFC based on Fe-based cathode catalyst (Acta 4020, 3.0 $mg_{catalyst}$ cm^{-2}), PdAg/CNT anode (0.5 $mgPdcm^{-2}$), and a Tokuyama A901 membrane delivered a power density of 0.245 W cm^{-2} at 80 °C [46]. A DG-AEMFC (crude glycerol) generated 0.268 W cm^{-2} with a Fe–Cu–N_4/C cathode (Acta 4020, 3.0 mg catalyst cm^{-2}), PtCo/CNT anode (0.5 mg_{Pt} cm^{-2}), and a Tokuyama A901 membrane [52]. A Pt-free borohydride AEMFC delivered a 0.283 W cm^{-2} using $Co(OH)_2$-PPy-C cathode and anode catalysts and a co-impregnated PVA-AER membrane, with T_{cell} = 60 °C [12]. Table 1.1 summarized the components, conditions, and peak power densities delivered by several types of AEMFCs.

Table 1.1 Selected data of AEMFCs fuelled with H_2 and several organic molecules

AEMFC type	Fuel	Oxidant	Cathode	Anode	Membrane	T_{cell} (°C)	Peak power density (W cm^{-2})	Ref.
H_2/O_2	H_2	O_2	0.53 mg_{Pt} cm^{-2} Pt/C (40% wt. Pt/C)	0.67 mg_{PtRu} cm^{-2} (40% wt. Pt/C)	ETFE-based benzyltrimethylammonium-functionalized radiation-grafted alkaline AEM	60	1.40	[21]
H_2/O_2	H_2	O_2	0.4 mg_{Pt} cm^{-2} Pt/C	PtRu/C (50% mass Pt and 25% mass Ru) 0.40 mg_{Pt} cm^{-2} Pt loading	Benzyltrimethylammonium-type AEM	60	1.16	[60]
H_2/O_2	H_2	O_2	Ag/C (40 wt. % Ag, 1.0 mg_{Ag} cm^{-2}).	PtRu/C (50%wt Pt and 25%wt Ru) 0.4 mg_{Pt} cm^{-2}	ETFE-[poly(ethylene-co-tetrafluoroethylene)]-based radiation grafted (RG)	70	1.10	[22]
H_2/O_2	H_2	O_2	Pt/C (60 wt. %, 0.4 mg cm^{-2})	PtRu/C (60 wt. %, Ru atomic ratio: 20%, 0.4 mg cm^{-2})	Quaternary ammonia polysulfone (QAPS) with hydrophobic side chain backbone	60	1.00	[61]
H_2/O_2	H_2 (dry)	Air (<10 ppm CO_2)	Ag, 3.0 mg_{Ag} cm^{-2}	Pd/C-CeO_2, 50 wt. % CeO_2 and 50 wt. % Vulcan XC-72 carbon, Pd loading: 0.3 mg cm^{-2}.	Ion exchanged to hydroxyl form by soaking in NaOH	73	0.50	[26]
H_2/O_2	H_2 (dry)	Air (CO_2 free)	Silver-based alloy (3.0 mg cm^{-2})	Pd/Ni (1.5 mg cm^{-2} total metal loading, with 0.3 mg_{Pd} cm^{-2})	Quaternary ammonium-functionalized	73	0.40	[62]
H_2/O_2	H_2	O_2	m-FePhen-C (Fe/N/C with highly active Fe-Nx/C sites, 1.0 mg cm^{-2})	40 wt. % Pt/C, 0.5 mg cm^{-2} Pt loading	A901 membrane, Tokuyama	50	0.27	[63]

H_2/O_2	H_2	O_2	Fe-NMG (a type of Fe-N-C), 3.5 mg cm^{-2}	10 wt% Pt/C, 0.2 mg cm^{-2}	A201 membrane, Tokuyama	70	0.22	[7]
H_2/O_2	H_2	O_2	CoPPY/C based, 2 mg cm^{-2}	Ni-W, 17.5 mg cm^{-2}	Quaternary ammonium-functionalized	60	0.040	[64]
DM	4 M KOH + 5 M CH_3OH	O_2	Fe_2O_3/Mn_2O_3(3:1)	PtRu/C (60 wt. %, 5 mg cm^{-2})	Polymer fiber membrane	60	0.046	[65]
DM	4 M KOH + 2 M CH_3OH	Air	MnO_2/C catalyst mixed with BP2000 carbon black (MnO_2: BP2000 = 1:1)	PtRu/C (70 wt. % Pt: Ru = 1:1 at. ratio, 4 mg cm^{-2})	Quaternized poly(vinyl alcohol)/poly(epichlorohydrin)	25	0.022	[66]
DM	8 M KOH + 2 M CH_3OH	Air	MnO2/BP2000	PtRu/C (70 wt. % Pt: Ru = 1:1 at. ratio, 4 mg cm^{-2})	Poly(vinyl alcohol)/ hydroxyapatite	25	0.011	[67]
DM	4 M KOH + 5 M CH_3OH	O_2	Mesoporous 3D N-doped yolk-shelled carbon spheres (Fe-N-C)	PtRu	Polymer fiber membrane	60	0.141	[68]
DE	2 M KOH + 2 M C_2H_5OH	O_2	Fe-N-C (from Fe(II)-phthalocyanine)	Pt-Ru/C (45 wt. %, 1.33 mg cm^{-2})	KOH-doped PBI membrane	90	0.062	[8]
DE	2 M KOH + C_2H_5OH 10 wt. %	O_2	Fe-Co/C, 2 mg cm^{-2} (C = Ketjen Black EC 600 JD, 1.13 wt. % Fe and 1.71 wt. % Co)	Pd/TNTA-web type (6 mg_{Pd} cm^{-2}, Ti web as the electrode support)	A201 membrane, Tokuyama	80	0.335	[45]
DEG	6.0 M KOH + 3.0 M $C_2H_6O_2$	O_2	Fe-based cathode catalyst (Acta 4020, 3.0 $mg_{catalyst}$ cm^{-2})	PdAg/CNT anode (0.5 mg_{Pd} cm^{-2})	A901 membrane, Tokuyama	80	0.245	[46]
DG	6.0 M KOH + 3.0 M crude $C_3H_8O_3$ (88 wt. %)	O_2	Fe–Cu–N_4/C cathode (Acta 4020, 3.0 mg catalyst cm^{-2})	PtCo/CNT anode (0.5 mg_{Pt} cm^{-2})	A901 membrane, Tokuyama	80	0.268	[52]
DB	5 wt. % $NaBH_4$ + 10 wt. % NaOH	O_2	$Co(OH)_2$-PPy-BP (3 mg cm^{-2})	$Co(OH)_2$-PPy-BP (5 mg cm^{-2})	Co-impregnated poly(vinyl alcohol)-anion exchange resin composite membrane	60	0.283	[12]

1.4 Advances in Membranes for PEM and AEM Fuel Cells

Fuel cells using polymeric membranes as electrolytes are most promising fuel cell technologies to provide clean, efficient, and energy dense power sources. Acidic proton exchange membrane (PEM) and alkaline anion exchange membrane (AEM) for applications in low temperature polymer electrolyte fuel cells will be reviewed in this chapter. Technically, both PEMFCs and AEMFCs operate with hydrogen at the anode and oxygen or air at the cathode, however, as PEM and AEM electrolytes transport different ions: acidic proton H^+ and alkaline OH^-, respectively, the resulting electrochemical reactions occurring are unlike, resulting in very distinct ions and water transport properties during fuel cell operation.

As illustrated in Fig. 1.4a, in PEMFC and AEMFC ions and water are not transported in the same directions. Water is generated at the anode (twice as much as in a PEMFC, per electron), and consumed at the cathode in AEMFCs which is fundamentally different to what occurs in PEMFCs [6]. These differences provide each technology with advantages and challenges.

PEMFC is a mature technology capable of producing extremely high-power densities, with the required durability for automotive and stationary applications. It has already penetrated many demanding commercial markets (e.g., backup power, materials handling, automotive including cars, trucks, and buses). However, it still depends on the utilization of costly platinum group metal (PGM) catalysts, perfluorosulfonic acid (PFSA)-based electrolytes, and pure hydrogen.

As a consequence of the expected market growth, PEMFCs will experience ever greater demands on cost, performance, and durability. In general, alkaline media provides a less corrosive environment to the catalysts, and the ORR kinetics is more rapid in alkaline media than in acidic media (Fig. 1.4b) [69].

This could potentially facilitate, in the case of AEMFCs, the use of less expensive non-platinum group metal (PGM) catalysts which expands the parameter space for

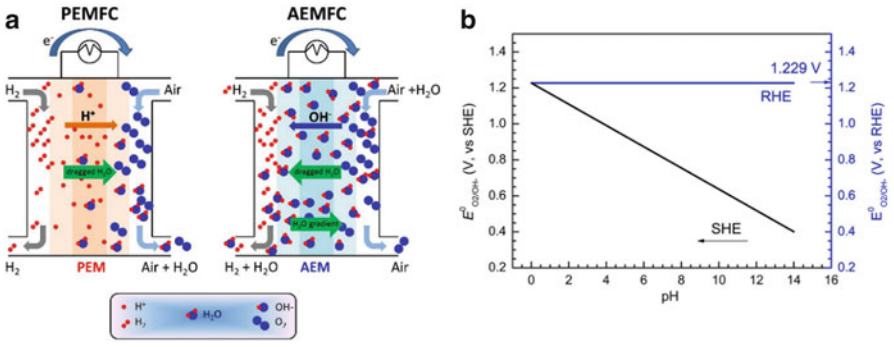

Fig. 1.4 (**a**) Schematic representation of an AEMFC as compared to a PEMFC (reproduced from Ref. [6] with kind permission of © Elsevier). (**b**) RHE scales with SHE of O_2/OH^- redox couple at different pH values of aqueous solutions (reproduced from Ref. [69] with kind permission of © Elsevier)

the discovery of highly selective catalysts with high stability in alkaline environments, and opens the possibility to consider hydrogen fuels containing substantial amounts of impurities. The foreseen cost reduction related to a possible free PGM catalysts fuel cell technology explains the resurgence of a large interest from industry and R&D community in AEM in the last decade. The following sections will introduce the state-of-the-art PEM and AEM and review recent development for both polymer electrolytes.

1.4.1 Proton Exchange Membranes (PEMs)

PEMs are solid polymer electrolyte membranes based on ionomers that contain fixed negative ionic functional groups, typically sulfonic acid (SO_3^-) and mobile positively charged cations, protons (H^+) in this case. PEMs are divided into three main categories: perfluorinated, semi-fluorinated, and hydrocarbon based.

Perfluorinated PEMs From a technology point of view, the development of perfluorinated sulfonic acid (PFSA)-based polymer membranes such as Nafion® has dominated due to their remarkable ion conductivity, low electronic conductivity, and chemical–mechanical durability compared to semi-fluorinated and hydrocarbon-based ionomer membranes. Still other properties such as water transport through diffusion and electro-osmosis, and the ability to fabricate high-performance membrane and membrane-electrode-assemblies (MEAs) are important when considering performance in operating system. However, researchers are actively working on alternatives to circumvent their high cost, limited use in low-temperature PEMs, and necessity of reinforcement to secure the required mechanical durability. Even after decades of research, Nafion® still stands as the state-of-the-art solid electrolyte for most PEMFC applications. Nafion® PFSA is a random copolymer developed in the late 1960s by Dupont composed of a non-ionic semi-crystalline polymer backbone of polytetrafluoroethylene (PTFE) and a randomly tethered long side chain with a pendant $SO3^-$ ionic group (sulfonic acid fluoride vinyl ether).

The different nature of the backbone and the covalently bonded pendant sulfonic groups results in a phase separation, as can be observed in Fig. 1.5a [70], which is enhanced by solvation upon hydration of the sulfonic groups to form water-swelled diffusion channels embedded in the hydrophobic matrix as revealed in Fig. 1.5b [71]. It is this phase-separated morphology between hydrophobic backbone and hydrophilic side chains that provides Nafion® its unique ion and water transport properties.

Most of fundamental research carried out on Nafion® membranes relates ionomer structure to properties (transport, physical, electrochemical, etc.) including computational work on mesoscale models and molecular dynamics (MD) simulations, with the objective of generating new synthetic approaches based on the fundamental understanding generated. Extremely extensive literature exists and was recently reviewed by Kusoglu et al. [72]. The reader is referred to the papers along with a

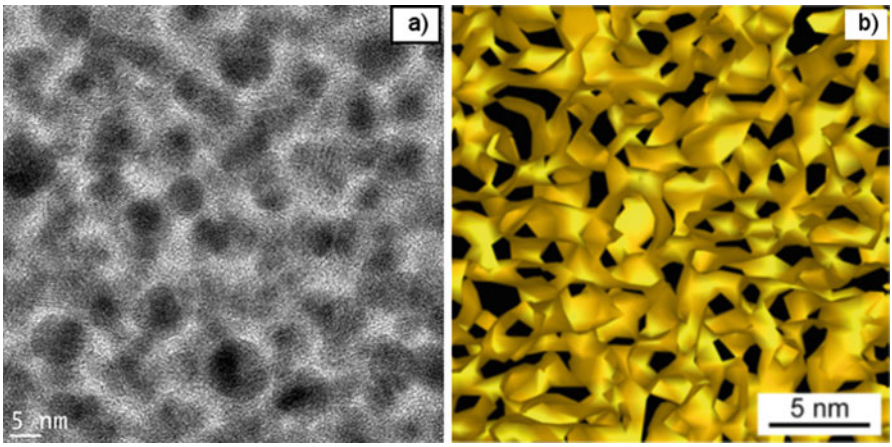

Fig. 1.5 (**a**) TEM on lead acetate stained Nafion® dry membranes. Ionic domains are dark (reproduced from Ref. [70] with kind permission of © The Electrochemical Society). (**b**) 3D reconstruction of the frozen hydrated cast Nafion membrane highlighting the spatial distribution of the hydrophilic domains in yellow (reproduced from Ref. [71] with kind permission of © The American Chemical Society)

number of other sources discussed. The most common synthetic approaches explored for new PFSA ionomers are based on the modification of either the backbone or side chain structure. The latest was mainly explored and generated several short side chain (SSC) ionomers, commercially available structures are illustrated in Fig. 1.6.

SSC-PFSA ionomers show higher structural crystallinity and increased glass transition temperature that translate to higher thermal stability compared to LSC-PFSA membranes. Furthermore, narrower ionic channels in SSC-PFSAs allow for improved water retention at low RH and lower gas crossover [73]. MD simulations suggest that shorter side chain ionomers have improved backbone flexibility, which enhances the proton dissociation and leads to higher conductivity [74, 75].

Modifications to the backbone length or distance between side chains resulted in smaller TFE repeat units and subsequently lower equivalent weight (EW) PFSAs. The EW being the mass of dry ionomer per mole of sulfonic acid groups, therefore lower EW ionomers show higher ion exchange capacity reaching IEC = 1.5 mmol/g for EW = 660 g/mol.

It was shown that due to the proximity of ionic groups in lower EW PFSAs, conduction mechanism may differ from LSC and may favor high temperature and low relative humidity operation, as supported by MD simulations [76]. Many studies intend to correlate side chain length and number of repeat units (or EW) to ionomers properties [77, 78]. There appears to exist a minimum backbone length or TFE repeat units $m = 3.5–5$ minimum for a PFSA to exhibit semi-crystallinity and the required packing order in the hydrophobic phase. Below this value, the ionomer exhibits a

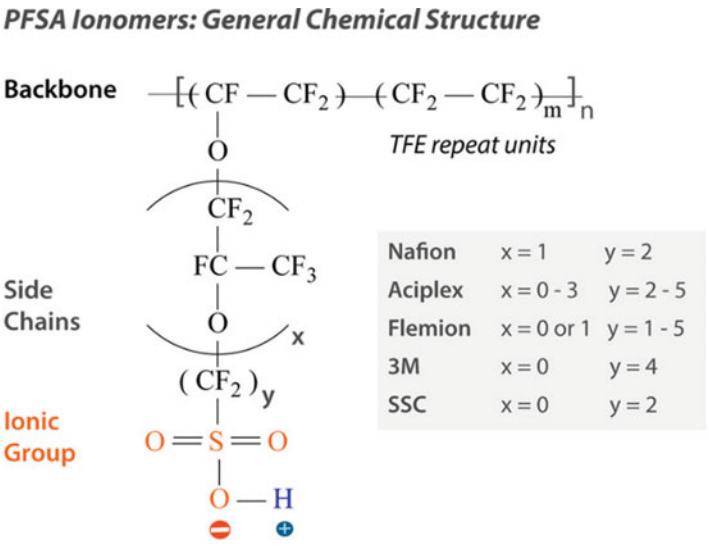

Fig. 1.6 PFSA ionomers general chemical structures (reproduced from Ref. [72] with kind permission of © The American Chemical Society)

gel-like behavior with weak stability, although with good proton transport properties. Studies reported minimum EW of 965 g/mol for Nafion® PFSA, 725 g/mol for 3 M PFSA, and 800 g/mol for Aquivion SSC-PFSA (previously Dow), which correspond to a minimum of 3–4 TFE units for all PFSAs [79–81].

PFSA ionomers offer a variety of PEMs which transport and mechanical durability among other properties, depend strongly on the TFE repeat units of fluorocarbon backbone, and the length of the sulfonic acid terminated side chains. The efforts to improve the transport functionalities and fuel cell performance are likely to compromise the mechanical durability and fuel cell longevity.

Besides increasing ionomers proton conductivity, another means to reduce proton resistance transport is to reduce membrane thickness, this strategy has led to the greatest improvement in PEMFC performance [82]. The advantages gained with this simple strategy include lower membrane resistance, improved hydration of the entire membrane, and lower material utilization and therefore, cost savings if we consider PFSA cost (e.g., 25 microns Nafion® 1100EW membranes cost vary between 1600 and 1300 US$/m^2 depending if reinforced or not). However, the extent to which a membrane can be thinned is limited, as gas crossover starts increasing, leading to increased voltage decay and earlier membranes failure.

PEMs manufacturing process could in some cases play an important role in compensating some of the mechanical weaknesses. Melt processes represent the best technologies to mass production of homogeneous thin polymer films at low cost. Besides eluding the serious safety and environmental concerns related to the mass production of membranes by solution-casting, melt processes provide a mechanical reinforcement through chain orientations following extrusion-stretching.

This structural reinforcement at a molecular level provides extruded PEM with the mechanical durability required for building robust and long-lasting PEM fuel cells, particularly for automotive applications. Mechanical degradation of three extensively studied model PFSA membranes was tested by Guittleman et al. [83] using humidity cycling tests: Nafion® NRE-211 (25 microns thick solution-cast membrane), Nafion® N111-IP (25 microns extruded membrane), and Gore-select® Series57 (18 micron e-PTFE reinforced three layers membrane). All membranes were made from LSC PFSA ionomer with EW = 1100, but prepared with different processes. Solution-cast membranes showed the shortest durability (4500 cycles), followed by e-PTFE-reinforced PEM (6000 cycles), extruded PEM has a significantly longer humidity cycling lifetime >20,000 cycles without failure. Significantly, even in model simulations, there appears to be a strong process-dependence of membrane morphology, indicating that structures produced by extrusion or solvent casting may be quite different, resulting in varied transport properties [76].

However, melt processing is only possible for ionomers that (1) possess the appropriate rheological properties to flow in the melt state and form uniform and mechanically sound thin membranes, and (2) are thermally stable at processing temperature. PFSA ionomers with sulfonic acid functional groups cannot be melt-processed as their melt processing temperature (>200 °C) is generally above sulfonic acid −SO3H groups degradation temperature. However, PFSA ionomers can be melt processed if the sulfonic acid functionality has been modified (i.e., sulfonyl fluoride precursor –SO_2F) or protected with additives to withstand melt processing high temperatures. In both cases a conversion of the membranes to the acidic form by hydrolysis or additive removal is required for operation in a fuel cell.

Extrusion by melt-casting, in the sulfonyl fluoride form followed by hydrolysis to convert to the sulfonic acid form, has been used to prepare proton exchange membranes, available commercially such as Nafion®N-117, Nafion®N-115, Nafion® N-1135, Nafion®N-112, and Nafion®111-IP with thicknesses of 183, 127, 89, 51, and 25 microns, respectively. These extruded membranes also suffer from anisotropy in their properties in general, generated by strong orientation in the machine direction that may cause a premature failure when submitted to humidity cycling in a fuel cell. Furthermore, the extrusion process by melt-casting does not allow the manufacturing of membranes thinner than 25 microns without compromising thickness uniformity.

It has been demonstrated that thermal stability of Nafion® PFSA ionomer is strongly dependent on the nature of the counterion associated with the fixed sulfonate site [84]. A number of small alkali metal and larger alkyl ammonium cation-exchanged Nafion® membranes were studied (e.g., sodium Na^+, potassium K^+, tetrabutylammonium TBA^+, tetramethylammonium TMA^+, tetradecylammonium $TDecA^+$) [85, 86]. It was found that Nafion® decomposition temperature is inversely dependent on the size of the exchanged cation, i.e., Nafion films show improved thermal stability as the size of the counter cation decreases. This inverse relationship of thermal stability with counterion size is strongly influenced by the strength of the sulfonate–counterion interaction. Most of the counterions investigated, even they

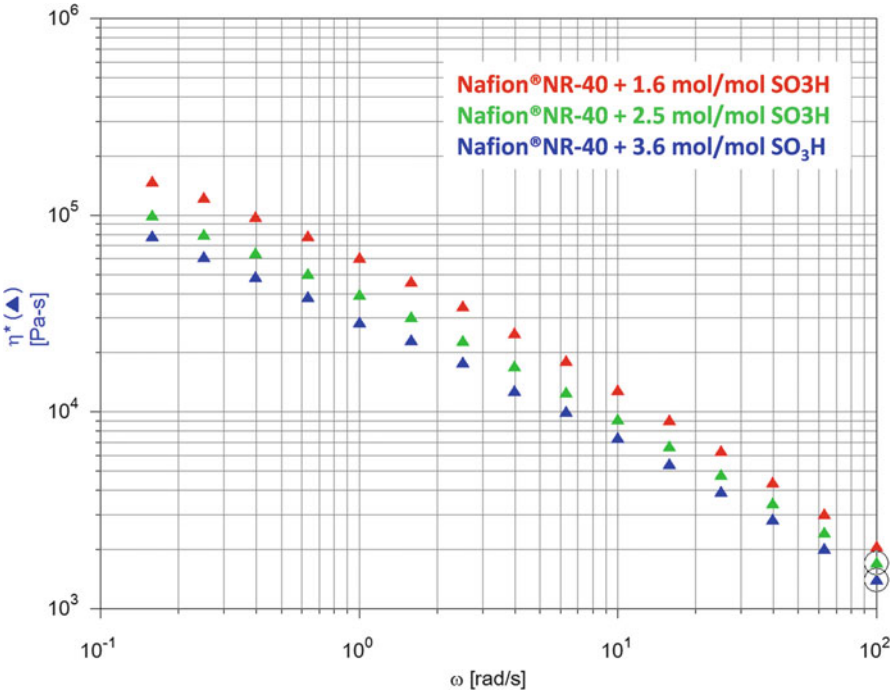

Fig. 1.7 Comparison of complex viscosity (η*) obtained from frequency sweep tests on Nafion® NR40 at 240 °C and different additive (1,2,4-triazole) content (from Ref. [89])

provided improved thermal stability of already processed membranes, do not allow for practical melt processing of PFSA ionomers.

Melt processing of LSC and SSC PFSAs in the acidic form using a series of heterocyclic azole molecules, i.e., benzimidazole, imidazole, and triazole, as additives was successfully investigated [87–89]. Figure 1.7 shows rheological data for Nafion® NR40 1000EW at 240 °C with different loading of 1,2,4-triazole, it shows the bifunctionality of the additive by neutralizing sulfonic acid groups on one hand, and acting as a plasticizer and aid-processing on the other. The complex viscosity is obviously reduced with increasing additive content.

Furthermore, PEMs were fabricated using an extrusion process based on melt-blowing of triazole neutralized Nafion® NR40 (EW = 1000). Some advantages of this process are (1) a better balance of mechanical properties than cast or extruded films because it is drawn in both the transverse and machine directions generating crystallinity in both directions, as a result mechanical properties of the thin film including tensile and flexural strength, and toughness are higher without e-PTFE reinforcement, (2) outstanding mechanical durability upon hydration and dehydration (>80,000 cycles) membranes swell preferentially in the thickness direction (Fig. 1.8 [89]) confirming that reduced in-plane swelling promotes long-term durability of the membrane electrode assembly (MEA) by constraining delamination of

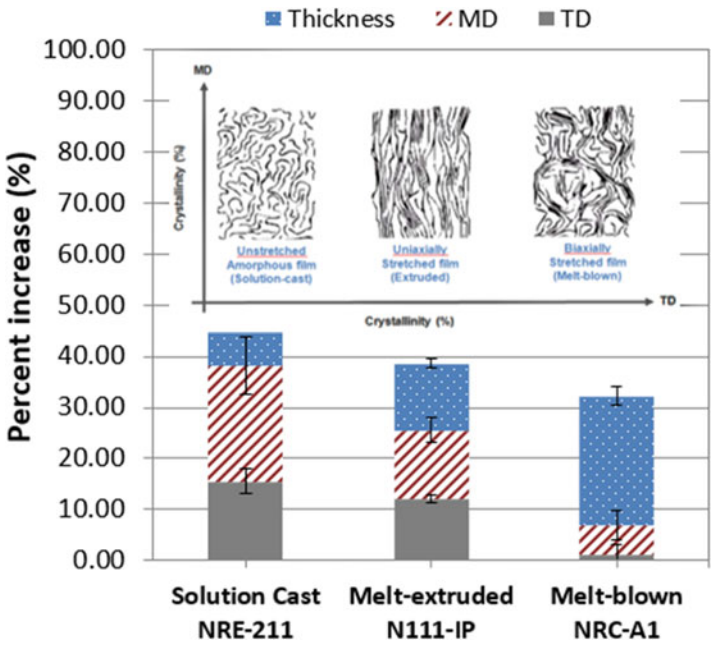

Fig. 1.8 Volume change for PEMs prepared with different processes as well as schematic representation of crystallinity evolution with processing. (From Ref. [89])

the catalyst layer from the membrane, (3) improved chemical durability; cumulative fluoride loss (CFL) was more than one order of magnitude lower than Nafion®NRE-211 reference; CFL = 160 mmol/cm^2 after 120 h (9.6 cycles) for the stack with Nafion®NRE-211 baseline and CFL = 5 mmol/cm2 after 162.5 h (13 cycles) for the five cell stack with triazole-Nafion®NR40 melt-blown membrane, and finally (4) PEM manufacturing cost is reduced 60–80% depending on annual production rates compared to e-PTFE reinforced solution-cast PEM.

Partially Fluorinated PEMs Non-fluorinated polystyrene sulfonic acid (PSSA) membranes were the first commercial polymer membranes developed in 1955 by GE [90] and were used in the first-ever operational PEMFC, the Grubb–Niedrach FC in the Gemini program. However, the system exhibited a short lifetime (<200 h) because of membrane poor stability and degradation under practical fuel cell operation, due to peroxide attacks on ternary benzylic hydrogen and the aromatic ring protons which results in IEC and conductivity loss, and membrane performance degradation. However, the very low cost of PSSA ionomer and its low fuel permeability originated the development of partially fluorinated PEM by substituting ternary hydrogen with fluorine resulting in more stable sulfonated poly(α,β,-β-trifluorostyrene) membranes developed by Ballard Advanced Materials as BAM3G membranes. These membranes contained sulfonated (α,β,-β-trifluorostyrene)- pendant groups and a perfluorinated backbone. Membrane

lifetime was strongly dependent upon equivalent weight and FC operating conditions, e.g., 3000 h operation time was achieved at 50 °C and low current density and only 500 h under practical FC conditions (higher current densities). A maximum operation time of 15,000 h was reported for pre-commercial BAM3G® [91, 92].

Radiation-induced grafting was largely investigated for the preparation of partially fluorinated polymers with styrene sulfonic acid (SSA) and modified SSA segments. Fluorinated polymers, such as polytetrafluoroethylene (PTFE), poly (tetrafluoroethylene-co-hexafluoropropylene) (FEP), poly(tetrafluoroethylene-co-perfluoropropyl vinyl ether) (PFA), polyvinylidenefluoride (PVDF), poly (vinylidenefluoride-co-hexafluoropropylene) (PVDF-co-HEP), poly(ethylene-tetrafluoroethylene) (ETFE), and polyvinylfluoride (PVF), were very stable and attractive skeleton structures for SSA-grafted membranes [93–99]. Such partially fluorinated grafted PEMs offered a substantially higher IECs with relatively moderate swelling because these membranes possessed isotropically connected ionic domains with high proton concentrations, PFEP-TFE-g-SSA membranes demonstrated proton conductivity up to 0.13 S/cm [100]. Unfortunately, these membranes exhibited substantially higher water absorption (up to 59 water molecules per SO_3 unit) than Nafion, which is a drawback as PEM materials. Another strategy to prepare SSA semi-fluorinated PEM was to blend polystyrene-based polymers with fluorinated polymers followed by post-sulfonation of styrene units [101, 102]. Polymer blending is one of the most effective methods to induce microphase separation. Despite all the strategies investigated, the applicability of partially fluorinated SSA-based membranes in PEMFCs is likely limited because the sulfonated styrene unit has a rather low oxidative stability even with fluorinated backbones or blends.

Poly(arylene perfluorocyclobutane) (PFCB), due to their particular thermal and chemical properties, are considered as high-performance partially fluorinated engineering materials for many applications [103–105]. The incorporation of proton-conducting groups in such macromolecular structures has been investigated for the development of PEM [106–110]. Various synthetic approaches were investigated and the most reported is based on the synthesis of functionalized bis-trifluorovinyl ether monomers, either in their sulfonic acid potassium salt form or as fluorosulfonyl analogues. Perfluorocyclobutyl (PFCB)-based blend PEM PFCB-based polymer blends comprising hydrophilic and hydrophobic polymers were prepared and characterized as PEM materials [109]. The hydrophobic polymers, BP-PFCB and SO_2-PFCB, were synthesized from the monomers 4,4′-bis(trifluorovinyloxy)-biphenyl 4,4′-sulfonyl-bis(trifluorovinyloxy)biphenyl, via a facile thermal polymerization. The hydrophilic blend component sBP-PFCB was prepared by the post-sulfonation of the BP-PFCB homopolymer using chlorosulfonic acid and thionyl chloride. The hydrophilic and hydrophobic components were combined in a common solvent obtaining transparent miscible membranes structurally stable with conductivities close to Nafion®.

Another PFCB copolymer developed through a collaboration between General Motors and Tetramer Technologies, LLC contains hydrophilic blocks of biphenyl vinyl ether (BPVE) with PFSA side chains and hydrophobic blocks of 1,1-bis

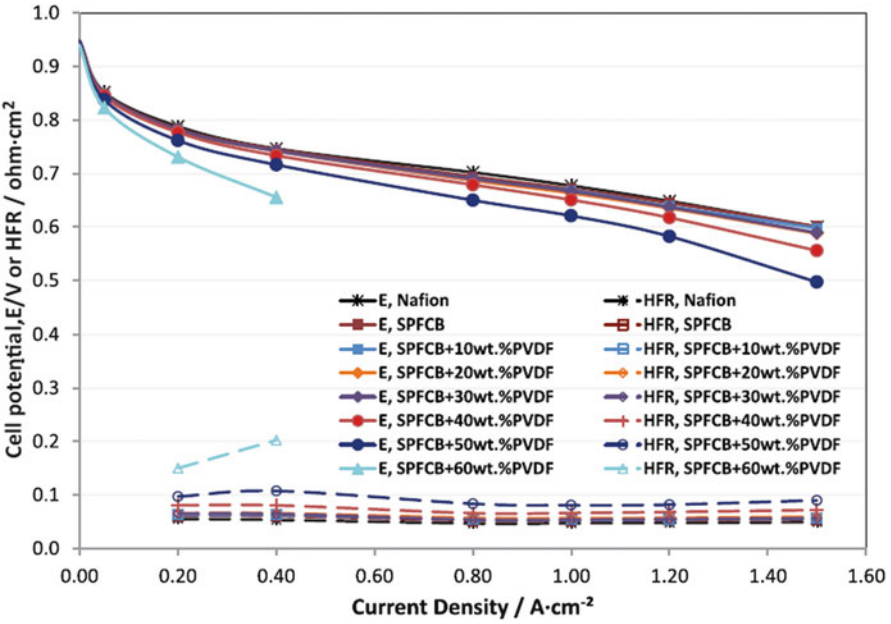

Fig. 1.9 Fuel cell polarization curves of MEAs containing SPFCB/PVDF blend membranes with various PVDF content (reproduced from Ref. [107] with kind permission of © Elsevier)

[4-[(trifluorovinyl)oxy]phenyl]hexafluoroisopropylidene (6F monomer) [107]. Proton exchange membranes based on SPFCB and SPFCB/PVDF blends with different PVDF contents (10–60 wt.%) were synthesized, fabricated, and characterized for fuel cell applications (Fig. 1.9) [107]. The composite SPFCB/PVDF membranes exhibit benefits of lower gas permeability and a higher ratio of conductivity to permeability compared to PFSA membranes for PVDF content <40 wt. %. In other work, e-PTFE-supported sPFCB membranes ran for over 3000 h in an accelerated durability test before ultimately failing due to chemical degradation [108]. This family of partially fluorinated PEMs based on SPFCB ionomer is probably one of the most promising alternatives to PFSA membranes because of the combination of good fuel cell performance, low gas permeance, and promising mechanical durability, as well as their relatively low projected cost.

Hydrocarbon PEMs Hydrocarbon-based PEMs are fluorine-free ion exchange membranes. This is probably the most investigated class of materials over the past few decades; they are of high interest because of their expected lower cost, intrinsically lower gas permeability, and higher glass transition temperatures compared to PFSA membranes. Most of hydrocarbon-based ionomers are sulfonated polymers and much of the research has focused on new (1) synthetic developments, (2) modification and functionalization of existing polymers, and (3) understanding of ionomers structures/properties relationship. Many publications covered extensive

reviews of all the strategies developed and the most relevant will be highlighted [111–114].

Hydrocarbon PEMs have been prepared from existing aromatic polymers and copolymers based on polystyrenes, polysulfones, polyimides, polyphosphazenes, polybenzimidazoles, poly(arylene-ether)s, poly(arylene sulfide)s, polyphenylenes, and many others. Polyarylene polymers and polymers containing phenyl pendant groups such as polystyrenes, as well as heterocyclic systems can be sulfonated by direct reaction with an appropriate sulfonating reagent. The most reactive sites for sulfonation depend on both the polymer structure and the directing effect of substituent groups. Simplicity and reproducibility were some of the advantages of polymers sulfonation, allowing for the possibility to generate different equivalent weights (EW) by controlling the reaction conditions. Most sulfonated polymers are thermally and mechanically stable up to 200 °C due to their more rigid polymer chain structure, and they have excellent fuel barrier properties, which lend themselves to PEM materials for low-temperature PEMFC applications. However, for a given IEC, sulfonated polymers generally have lower proton conductivities and higher dimensional swelling compared with PFSAs because of their lower acidity, lower hydrophobicity of polymer backbone, and weaker phase separation between hydrophilic and hydrophobic moieties, resulting in less effective microphase-separated morphology for water channel formation [113]. Furthermore, the starting polymers were originally developed for applications in environments different from those prevailing in a PEM fuel cell, i.e., temperature, relative humidity, pH, presence of radicals, etc. Under saturated vapor conditions, all materials (both sulfonated and non-sulfonated) show some decomposition between 150 and 200 °C, although the thermohydrolytic stability of the sulfonated polymers is always lower than that of the corresponding unmodified starting material, sulfonated polymers all show loss of sulfonic acid groups and hydrolysis of the functionalized units to some extent. Chemical stability of sulfonated polymers appears to be lower than PFSAs, particularly those with electron-rich structures containing ether linkages. As a general observation, sulfonated polyaromatic polymers are slightly more stable than sulfonated polyheterocyclic systems [111].

Sulfonated polymers can also be synthesized via various synthetic routes from diverse monomers to obtain a variety of structural architectures, e.g., random copolymer, block copolymer, grafted copolymer, and densely sulfonated or clustered copolymer. Synthetic routes provide the opportunity to have a better control of (1) the position and number of functional groups, which in turn define the ion exchange capacity and the morphology (hydrophobic/hydrophilic phase separation), and (2) the molecular weight to enhance durability which is more difficult to achieve with post-reaction on existing commercial polymers. The characteristics of functional groups such as position on the polymers chains (e.g., main chain, pendent unit, side chain, etc.), flexibility, and acidity or basicity are also important in the control of the final ionomer's morphology [112, 114]. The polymer backbone characteristics such as size, stiffness, hydrophobicity, and electron-withdrawing or -donating effects influence the hydrophobic domain structure.

Compared with random copolymers, block copolymers induce more ordered microphase-separated morphology because the different characteristics and length of each block induced phase separation. The chemical structure of hydrophobic sequences is one of the critical factors leading to phase separation. Furthermore, oligomer block lengths influenced the morphological features and interdomain distances. Longer block lengths induced clearer phase separation and increased domain sizes.

Various types of hydrocarbon-based ionomer membranes have been proposed for application in fuel cells, many studies reported ionic conductivities and even fuel cell performances higher than PFSAs, however, the issue of chemical and mechanical degradation of this class of ionomer membranes, especially under automotive operating conditions, has not been fully resolved at present. Shimizu et al. [115] reported recently on the chemical durability of two proton-conducting hydrocarbon polymer electrolyte membranes based on sulfonated benzophenone poly(arylene ether ketone) (SPK) and sulfonated phenylene poly(arylene ether ketone) (SPP) semiblock copolymers using accelerated OCV stress testing. Even if SPP-based fuel cell showed slower OCV decay compared to SPK, both hydrocarbon PEMs exhibited remarkable stability compared to Nafion®NRE211 baseline (Fig. 1.10.). They suggested that the lower hydrogen permeation in the cell led to a decreased

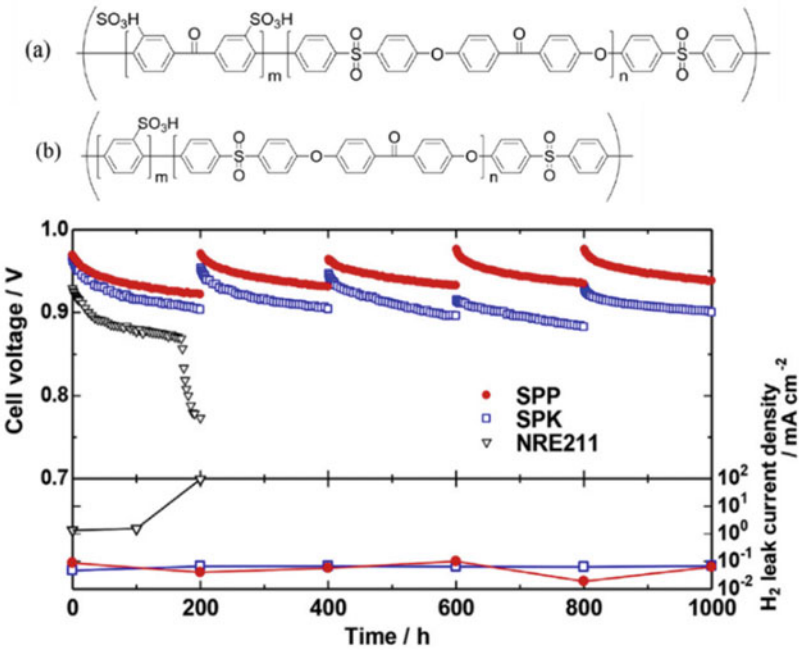

Fig. 1.10 Chemical structure of (**a**) sulfonated benzophenone poly(arylene ether ketone) (SPK) (**b**) sulfonated phenylene poly(arylene ether ketone) (SPP) semiblock copolymer, and cell voltage decay and hydrogen leak current density (reproduced from Ref. [115] with kind permission of © Elsevier)

production of oxidative radical species generated at the anode and led to a slowing of membrane degradation kinetics.

After decades of R&D and despite the progress made, the limitations related to the mechanical and chemical durability are still to be addressed for hydrocarbon PEMs to become suitable alternatives to perfluorinated fuel cell membranes, and simultaneous mitigation mechanisms for chemical and mechanical degradation should be mutually compatible. Gubbler et al. suggested that the shortcomings related to the mechanical durability should be solved using approaches that both reduce the membrane stress during humidity cycling and increase the strength at dry conditions, for instance, by minimizing in-plane swelling via clever multi-block copolymer architectures and lowering membrane stiffness by blending or copolymerizing with elastomeric polymers [108]. Membranes manufacturing process can also be an effective way for achieving low in-plane swelling when possible [89]. The approach effectively used for PFSA PEMs is to simultaneously reduce in-plane swelling and increase strength by using a relatively stiff porous e-PTFE polymer support. Radical induced chemical degradation will require a dedicated antioxidant strategy that needs to be self-sustaining over thousands of operating hours.

1.4.2 Anion Exchange Membranes (AEMs)

AEMs are solid polymer electrolyte membranes that contain fixed positive ionic groups, typically quaternary ammonium (QA) functional groups, and mobile negatively charged anions usually hydroxide (OH^-). As there are no typical membranes comparable to Nafion® used in PEMFCs, the development of an AEM equivalent to the well-established perfluorosulfonic acid proton exchange membranes (PEM) in their hydroxide form is hindered by several issues, the most reported are: (1) low intrinsic ionic conductivities; typical quaternary ammonium ionic groups in AEM are less dissociated than the typical sulfonic acid groups (pKa for sulfonic acid groups are typically -1 but for QA groups the related pKb values are around +4); [116] the diffusion coefficient of OH^- ions is twice less than that of H^+ (in bulk water), a higher concentration of OH^- ions is needed to achieve similar results, which in turn requires higher ion exchange capacity of the polymer. Achieving OH^- ion conductivity comparable to H^+ conductivity observed in PEMFCs becomes challenging without compromising mechanical properties due to excessive swelling, (2) the molecular structure of the membrane itself decomposes due to the presence of the highly nucleophilic OH^-. Decomposition typically starts at temperatures above $T = 60\ °C$ and leads to a reduction of ion exchange capacity (IEC), conductivity, and mechanical strength, and (3) the OH^- in AEMs is readily converted into carbonates when in contact with ambient CO_2 that precipitate irreversibly compromising electrodes porosity and fuel cell durability [117, 118].

The increased number of studies in the past few years indicates a growing interest in the research community, driven by the several advantages that AEMFC technology

might deliver over the currently commercialized proton exchange membrane fuel cells (PEMFCs) as mentioned at the beginning of this chapter. Improvements in the past decade show that newly developed AEMs have already reached high levels of conductivity, leading to satisfactory cell performance [6]. The most common, technologically relevant backbones reported are poly(arylene ethers) of various chemistries such as polysulfones (including cardo (polymer molecule with cyclic side groups whose one of the atoms belongs to the main polymer chain, phthalazinone, fluorenyl), poly(ether ketones), poly(ether imides), poly(ether oxadiazoles), polyphenylenes and poly-(phenylene oxides), polybenzimidazoles, poly(epichlorohydrins), unsaturated polypropylene and polyethylene, polystyrene, poly-(vinyl alcohol), poly(vinylbenzyl chloride), polyphosphazenes, perfluorinated, and based organic and inorganic hybrid types. Also, methods of preparation, including synthesis, radiation-grafting, plasma synthesis, pore-filling, electrospinning, and PTFE-reinforced types, have been reported [119]. The cationic functional-group chemistries that have been studied include (1) N-based groups, such as quaternary ammoniums (QA), heterocyclic systems (including imidazolium, benzimidazoliums, and pyridinium), guanidinium systems, (2) P-based types including stabilized phosphoniums, (3) sulfonium types, and (4) metal-based systems.

Although alternative cationic species from phosphonium or sulfonium groups have been shown to be less stable than QAs with similar substituents, some potentially viable highly sterically shielded phosphonium groups may be relevant, however, their synthesis is highly complex [120, 121] which is the reason why current research efforts mainly focus on QAs as anion exchanging groups.

Alkaline stability of many different QA groups was investigated by Marino et al. [118] for temperatures up to 160 °C and NaOH concentrations up to 10 mol/L with the aim to provide a basis for the selection of functional groups for AEMs. Most QAs exhibit unexpectedly high alkaline stability with the exception of aromatic cations. β-hydrogens are found to be far less susceptible to nucleophilic attack than previously suggested, whereas the presence of benzyl groups, nearby hetero-atoms, or other electron-withdrawing species promotes degradation reactions significantly. It is to remind that Hofmann elimination when β-hydrogens are present and direct nucleophilic attack by OH^- ion at the cationic site were for long time the most suggested AEM degradation mechanisms. Cyclic QAs proved to be exceptionally stable, with piperidinium-based cation featuring the highest half-life at the chosen conditions (Fig. 1.11).

Overall the degradation rate of quaternary ammonium (QA) groups increases dramatically both with OH^- concentration and temperature. It is important to mention that ex-situ alkali stability tests may not be necessarily representative of the AEMs stability in real fuel cell systems, where the membranes have to endure dehydration cycles [19] and might show reduced stability. This shows the importance of sufficient hydration of AEMs in alkaline fuel cells for achieving long durability.

A large number of AEMs have been synthesized using different combinations of polymer backbones and cationic functional groups for AEMFC. The results have been compiled over the last decade for different functional groups. An increasing

Table 1. Half-life of QA compounds at $T = 160\,^{\circ}C$ in 6 M NaOH with electron-withdrawing and electron-donating substituents compared to a neutral BTM, BTE, and the TMA benchmark (entries 1–5) and DABCO- (entries 6 and 7) and piperidinium-based QAs (entries 8 and 9) with and without a benzylic group.

Entry	QA	Abbreviation[a]	Half-life [h]
1		TMA	61.9
2		MBTM	16.6
3		BTM	4.18
4		BTE	0.68
5		NBTM	0.66
6		MAABCO	13.5
7		BAABCO	1.4
8		DMP	87.3
9		BMP	7.3

[a] TMA: tetramethylammonium; MBTM: 3-methoxy-benyzl trimethyl ammonium; BTM: benzyltrimethylammonium; BTE: benzyltriethylammonium; NBTM: 3-nitrobenyzltrimethylammonium; MAABCO: 1-methyl-4-aza-1-azonia-bicyclo[2.2.2]octane; BAABCO: 1-benzyl-4-aza-1-azonium-bicyclo[2.2.2]octane; DMP: *N,N*-dimethylpiperidinium; BMP: *N*-benzyl-*N*-methylpiperidinium.

Table 2. Half-lifes of BTM and various aromatic QA compounds at different temperatures in 6 M NaOH.

Entry	QA	Abbreviation[a]	Half-life [h]	*T* [°C]
1		BTM	4.18	160
2		PhTM	0.14	160
3		TMI	too short to measure	160
4	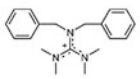	DTG	too short to measure	160
5		MOI	too short to measure	60
6	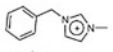	BMI	too short to measure	25
7		BP	too short to measure	25

[a] PhTM: phenyltrimethylammomnium; TMI: 1,2,3-trimethylimidazolium; DTG: 1,1-dibenzyl-2,2,3,3-tetramethylguaninidinium; MOI: 1-methyl-3-octylimidazolium; BMI: 1-benzyl-3-methylimidazolium; BP: *N*-benzylpyridinium.

Fig. 1.11 Half-life of quaternary ammonium (QA) compounds in 6 M NaOH (reproduced from Ref [118] with kind permission of © Elsevier)

number of studies succeeded to show good performance from cells made of improved materials developed for AEMFC technology. Pan et al. [19] made a comprehensive review and compiled fuel cell performance. Figure 1.12 shows performance and stability data for some of the best performing AEM.

The highest performance obtained was for AEM based on vinylbenzyl chloride (VBC) radiation grafted onto poly(ethylene-cotetrafluoroethylene) (ETFE) films followed by amination with trimethylamine that shows a very impressive peak power density of 1.4 W/cm^2. Nevertheless, and in spite of the many published reports with AEMFC performance test data, there are only a very few research studies reported in the literature of AEMFCs showing performance data of cells completely free of Pt (in both anode and cathode) and very few studies on cell performance stability which remains a challenge for the commercialization of AEMFC technology.

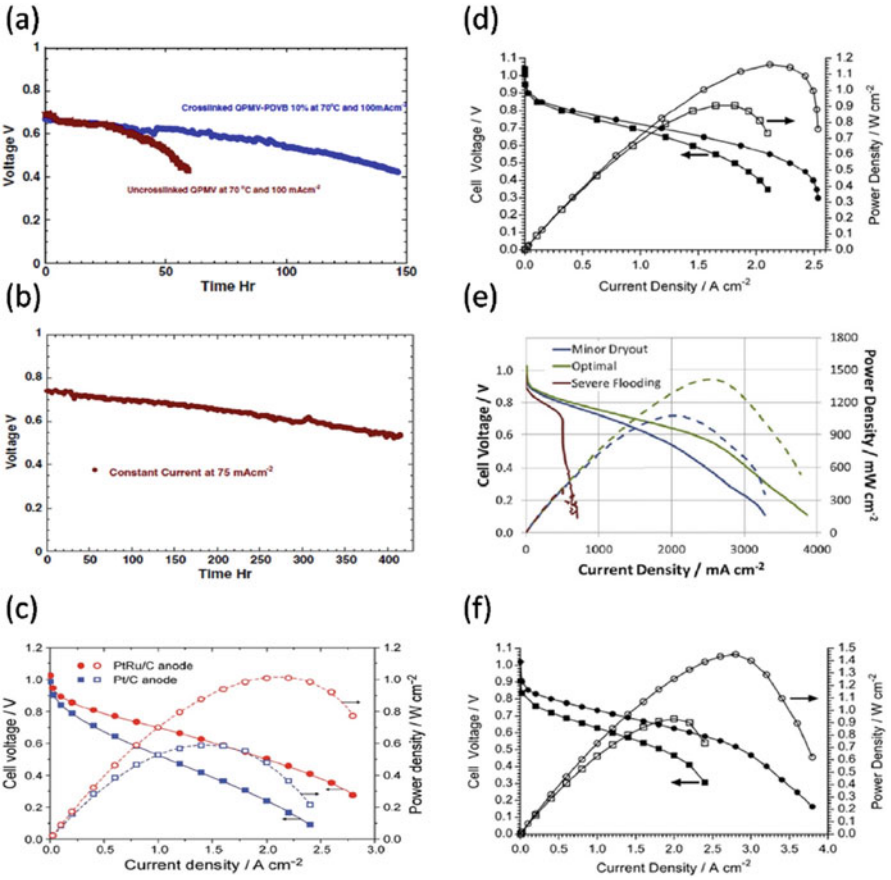

Fig. 1.12 Best performing H_2-AEMFCs from recent literature (reproduced from Ref [19], kind permission of © Elsevier). (**a**) Durability tests of uncrosslinked QPMV and 10% crosslinked QPMV-PDVBAAEM at 70 °C. (**b**) Durability test of 10% crosslinked AAEM at 50 °C [122]. (**c**) Cell performance of the AEMFC using the PtRu anode or Pt anode [61]. (**d**) Performance of H_2/O_2 AEMFC test data at 60 °C for E-R (squares) and E-6 (circles) using PtRu/C anodes and Pt/C cathodes and with no gas back-pressurization of the fully humidified gases [60]. (**e**) Performance of the AEMFC with different hypothesized distribution of water across the AEM and electrodes in an AEMFC [21]. (**f**) Performance of H_2/O_2 AEMFC at 80 °C with the LDPE-AEM with Pt/C (circles) or Ag/C (squares) as cathodes as well as PtRu/C anode [123]. (**a**, **b**, **e**: reproduced with kind permission of © Elsevier; **c**, **d**, **f**: reproduced with kind permission of © The Royal Society of Chemistry)

Finally, for all ionomers developed for PEM or AEM application, composite or blend membranes have been studied extensively in an attempt to compensate for some of the disadvantages of purely polymeric membranes. Functionalized or non-functionalized inorganic fillers have been incorporated to provide additional ions acceptor/donor sites, bind and retain water molecules at higher temperature, enhance ionic conductivity, improve mechanical properties, or have radical

scavenging effect to extend membranes lifetime. Polymer blending is also a promising method for inducing a microphase separation in membranes, controlling the swelling, and reinforcing mechanically the ionomer. In both cases compatibility of composite and blend materials with the host ionomer is critical.

1.5 Electrocatalytic Reactions in Proton Exchange Membrane (PEM) Fuel Cells

The operation of proton exchange membrane fuel cells (PEMFC) is based on the electrochemical reactions which occur at the interface "catalytic layer-electrolyte.". These reactions are the oxidation of the fuel at the anode and the reduction of the oxidant at the cathode. In practice, the electric efficiency of fuel cell depends on the current density j delivered by the cell. This efficiency is lower than that of the equilibrium reversible at $j = 0$ because of the irreversibility of the electrochemical reactions at the electrodes. Therefore, the cell voltage E_{cell} at $j \neq 0$ is expressed as follows:

$$E_{\text{cell}}(j) = E^{\circ}_{\text{eq}}(j = 0) - (|\eta_a| + |\eta_c| + R_e|j|) \tag{1.24}$$

where R_e is the cell resistance, $E^{\circ}_{\text{eq}}(j = 0)$, the cell voltage at $j = 0$, η_a and η_c are the overpotentials at the anode and the cathode, respectively.

It clearly appears that lower is the overpotential value better is the cell voltage. Therefore, progress in fuel cell is mostly focused on the decrease of the overpotential at the electrode and improves considerably the activity by developing new type of materials. In addition, the decrease of the electrode materials cost is a challenge since most of active materials are expensive noble metals mainly the platinum group metals.

Since this discovery, progress and improvements in this system were possible due to the innovations in various domains (nanotechnology, mechanical engineering, chemistry, electrochemistry, fluid management, etc.) which permitted to enhance substantially the performance of the cells. The last 30 years, the metal loading in the catalytic layer of PEMFCs has been divided by more 100. This improvement was due to the amazing progress in nanomaterials fabrication and also in the engineering of producing membrane electrodes assemblies (MEA). During the two last decays, various methods (chemical and physical) were adapted for elaborating very fine disseminated nanoparticles on the usual carbon support [124]. In addition, different types of carbon (such as carbon nanotubes, porous carbon, and recently graphene) were proposed as a support for nanocatalysts in order to avoid the corrosion and to improve the electron transfer observed on the usual carbon Vulcan XC 72 or 72R during the cell operation.

At the anode, various compounds can be used as fuel in PEMFCs. Up to date the operation conditions of the proton exchange membrane fuel cells have permitted to

investigate the hydrogen, formic acid, and various alcohols such as methanol, ethanol, glucose, hydrogen but also the formic acid and some alcohols.

1.5.1 Reactions of Fuel at the Anode of PEMFCs

1.5.1.1 Case of H_2

Hydrogen appears as the greenest fuel since its oxidation leads to water and heat. Under acidic environment, the H_2/O_2 fuel cell operates with the electrooxidation of H_2 at the anode and the oxygen reduction reaction at the cathode. It is well known that the kinetics of hydrogen oxidation reaction (HOR) is very fast mainly on platinum electrode. The half-cell reaction is as follows:

$$H_2 \rightarrow 2H^+ + 2e^- \qquad E^\circ = 0.000 \text{ V vs.SHE} \tag{1.25}$$

At the interface of the anode, the formed protons diffuse by migration through the polymer electrolyte membrane to the cathode where they react with the oxygen to produce water. In electrocatalysis, this reaction is taken as a model to explain mechanism of adsorption/desorption, diffusion, since it involves one electron per hydrogen atom. The overpotential η_a observed for the H_2 electrode is very small. Thereby, it can be approximated by the linear relationship with j as follows: $\eta_a = R_t j$, where R_t is called the charge transfer resistance [125].

Due to its presence at the anode of H_2/O_2 fuel cell, the HOR is deeply studied for understanding the different pathways when the reaction occurs on Pt electrodes. A pioneer work was done at the end of 1980s by Ticianelli et al. [126] with high metal loading (as 4 $mg_{Pt}\,cm^{-2}$) in a complete H_2/O_2 cell. Presently only few $\mu g_{Pt}\,cm^{-2}$ are enough to reach a highest cell performance [127, 128]. The study of HOR requires RDE measurements. Extensive study of this reaction was made by Croissant et al. [129] with different metal loadings from 0 to 0.3 $mg_{Pt}\,cm^{-2}$. These authors demonstrated the catalyst loading of 150 $\mu g\,cm^{-2}$ is the maximum value which below the evolution of the exchange current density is linear.

The reaction (1.25) can be expressed in three elementary reaction steps:

$$H_2 + \ 2\,Pt \leftrightarrow 2\,H_{ads} - Pt \qquad \text{Tafel reaction} \tag{1.26}$$

$$H_2 + Pt \leftrightarrow H_{ads} - Pt + H^+ + e^- \qquad \text{Heyrovsky reaction} \tag{1.27}$$

$$H_{ads} - Pt \leftrightarrow Pt + H^+ + e^- \qquad \text{Volmer reaction} \tag{1.28}$$

where H_{ads} is the adsorbed hydrogen atom as an adatom.

The dissociative adsorption of a hydrogen molecule is followed by two separate one-electron oxidations of the H_{ads} in the case of Tafel–Volmer pathway, while for the Heyrovsky–Volmer pathway, two one-electron oxidation occur. The first one is held simultaneously with chemisorption and the second one is the oxidation of H_{ads}.

To explain the HOR current behavior in the entire overpotential region relevant to the reaction, Wang et al. [130] have developed a dual-pathway kinetic equation which fits perfectly with the high surface electrocatalysts operating at 80 °C in fuel cells conditions.

Despite the simplicity of the HOR, efforts have been made for modelling the reaction, decreasing the amount of the Pt loading, or for elaborating new and very active catalyst tolerant for CO. Indeed, more than 80% of the hydrogen produced come from partial oxidation or steam reforming of hydrocarbons. Thereby, H_2 produced from this process contains traces of CO. CO is also one of intermediates from the oxidation of organic molecules (methanol, ethanol, etc.) on Pt electrode [131]. CO molecule strongly adsorbs on the Pt active sites and greatly decreases the performance of the Pt anode in fuel cell. Therefore the oxidation of CO is one of the mostly studied reactions in electrocatalysis due to the poisoning effect observed. Two approaches are possible to oxidize CO molecule on Pt electrode: (1) apply a high potential, or modify the structure and the composition of Pt in order to oxidize CO at very low potential. This second approach is suitable for the operation conditions of fuel cells. Considering Eq. (1.29), CO molecule requires an external oxygen for its complete oxidation in acid medium. Therefore, electrochemists added to Pt a second metal able to provide oxygenated species at very low potentials.

$$CO + H_2O \rightarrow CO_2 + 2H^+ + 2e^- \tag{1.29}$$

Figure 1.13 shows the effect of Ru and Sn added to platinum on the oxidation of CO. Pt-Sn electrode oxidizes CO at a potentials values 600 mV lower than that of Pt bulk electrode.

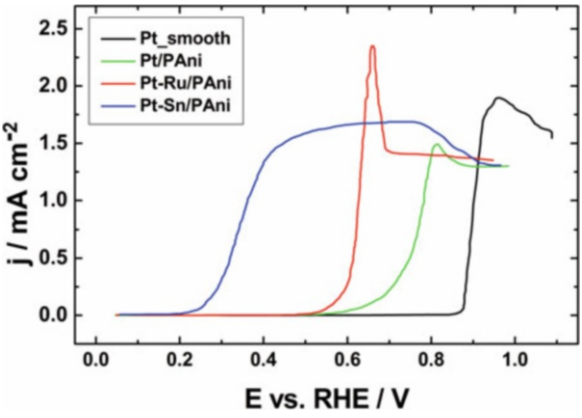

Fig. 1.13 Positive scan during the oxidation of CO on various Pt-based catalysts disseminated in a 0.5 µm thick of polyaniline film recorded in $HClO_4$ 0.1 moles L^{-1}, at room temperature and at 5 mV s^{-1}

1.5.1.2 Case of CH_3OH

The kinetics of alcohols oxidation on Pt in acid medium is low and leads to the formation of intermediates strongly adsorbed on the active sites. Therefore, the oxidation of some alcohols (i.e., methanol and ethanol) becomes the aim of several investigations in electrocatalysis.

For the some mobile applications of PEMFCs, H_2 is not suitable to hand and a liquid fuel appears the suitable solution. Therefore, organic fuels such as alcohols (i.e., methanol and ethanol) are proposed. However, the kinetics of their oxidation reactions is very slow because of the low operating temperature of the PEMFCs and the several steps involved. The oxidation of such alcohols occurs with very high overvoltages η_a (Fig. 1.14). Therefore, the challenges at the anode are to considerably decrease these overvoltages as indicated in Fig. 1.14.

The complete oxidation of methanol to CO_2 in acid medium is:

$$CH_3OH + H_2O \rightarrow CO_2 + 6\,H^+ + 6e^- \tag{1.30}$$

This oxidation is a six electrons transfer process which leads to several intermediates as extensively stated in the literature [131, 132]. During the oxidation of methanol on Pt catalysts, the cleavage of C–H bonds leads to the formation of the so-called formyl-like species $-(CHO)_{ads}$. This species can give $-CO_{ads}$, $-COOH_{ads}$, or directly CO_2. For oxidizing at low potential these three species to CO_2, or to avoid their formation, effective catalysts are needed. For promoting the oxidation of CH_3OH and its intermediates at low potential, other metals (Ru, Sn, Mo, Ni, Mo, etc.) are added to platinum to promote the formation of oxygenated species at low potentials [131–142]. Indeed, these metals can be oxidized at relatively low

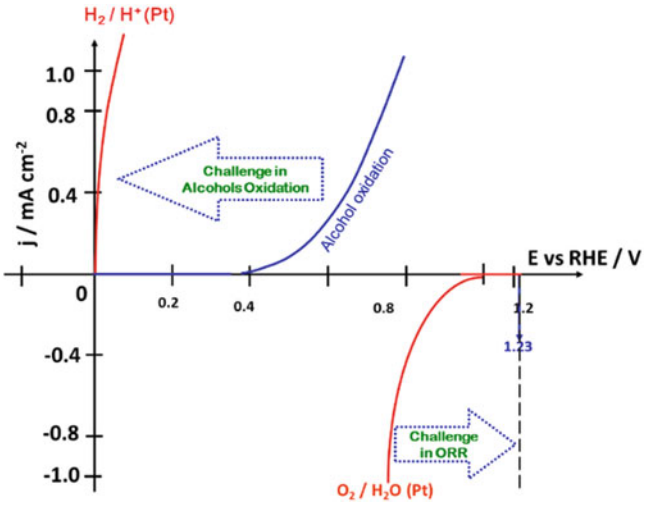

Fig. 1.14 Schematic drawing of the challenges at the electrodes of PEMFCs

potential. These materials activate and dissociate H_2O molecule while the organic molecule is adsorbed on Pt. Then a surface reaction involves the oxygenated species from the second metal and the organic adsorbed species will lead to the formation of CO_2. This surface reaction is known as a bifunctional mechanism which was suggested by Watanabe and Motoo [131, 143]. The structure, composition, and support of electrocatalyst are some parameters which are still studied for improving their performance towards the oxidation of methanol [132–146].

1.5.1.3 Case of CH_3CH_2OH

Ethanol is an attractive molecule which can be used directly in PEMFC system named direct ethanol fuel cell (DEFC). The complete oxidation of ethanol at the anode of DEFC is the following:

$$CH_3CH_2OH + 3H_2O \rightarrow 2CO_2 + 12\,H^+ + 12e^- \tag{1.31}$$

This reaction is complex since it involves theoretically 12 electrons transfer process which cannot be achieved in one step. The main challenge with this molecule is to break the C–C bond in order to complete the oxidation of challenge on this molecule is to the cleavage of the C–C bond. In reality, partial oxidation occurs leading to the two main products, the soluble acetaldehyde and the acetic acid. The reaction has been widely investigated mainly by in situ FTIR [147–149]. This technique permits to reveal the enhancement of catalysts. Up to now, Pt is the main element of electrode materials developed for the oxidation of ethanol. To avoid the partial oxidation pathway reactions, bi and trimetallic catalysts have been proposed [144, 147–183]. Pt-Sn/C is the electrode materials which exhibited high catalytic activity towards the oxidation of ethanol. However, a third element is required to improve the dehydrogenation reaction and also the cleavage of the C–C bond. The addition of Ni on PtRu/C and PtSn/C significantly increases the catalytic activity of these nanomaterials [177]. In the literature, various electrode materials have been proposed for the electrooxidation of ethanol, but few of them have a significant improvement compared to the platinum electrode. Effective electrocatalysts have to be developed.

1.5.1.4 Reaction at the Cathode: Oxygen Reduction Reaction (ORR)

The reaction which occurs at the cathode of all PEMFCs is the electrochemical reduction of molecular oxygen known as oxygen reduction reaction (ORR). In acid medium, the reaction is:

$$O_2 + 4H^+ + 4\,e^- \rightarrow 2H_2O \tag{1.32}$$

This reaction is complicated since it involves many intermediates which depend on the electrolyte, the nature, composition, and structure of electrode materials. The reduction of molecular oxygen in water involves four electrons. Damjanovic et al. [184] and later Wroblowa et al. [185] have made a pioneer investigation and suggested the mechanism explaining the different intermediates observed during the ORR. They pointed out the multi-electron transfer process and the main two-electron pathway which leads to the formation of hydrogen peroxide. According to the schematic drawing (Fig. 1.14), it appears that the ORR shows the sluggish reaction kinetics and the assessment of the intermediates is an important and key step for improving the catalytic performance of electrode materials. Several studies by rotating disk (RDE) and rotating ring disk (RRDE) electrodes have permitted to reach the kinetics parameters of the reaction on various catalysts [186–188]. The development of nanomaterials has permitted to improve the performance of the cathode materials due to their high surface to volume ratio. The most active material for ORR is platinum due to the bonding energy of some species like O and OH with its surface [189]. The RDE measurements are a useful technique for evaluating the electrocatalytic behavior of electrode materials for a reaction limited by the diffusion. It required three-electrode cell while for the RRDE, four electrodes system with a bi-potentiostat is required. Indeed, a part the reference and the counter electrodes, two working electrodes is needed. One (the disk) is the catalyst to be studied and the second (ring) to detect directly the amount of hydrogen peroxide produced during the reaction.

As ORR is limited by the diffusion, two conditions are needed to validate the Levich law: (1) the existence of a mass transport process that is the rate-determining step (rds), and (2) the reaction is of a first-order reaction with respect to the electro-reactive species (O_2). Afterwards, to apply the Koutecky–Levich equation, two conditions are required: (1) the existence of an electron transfer process that is the rate-determining step (rds), (2) the reaction is of a first-order reaction with respect to the electro-reactive species (O_2). The equations and the treatment of the data will not be exposed in this chapter. It is extensively detailed in the literature [188]. Figure 1.15 shows the polarization curves obtained for Pt and Pt-Cr/C catalysts in O_2 saturated acid medium and corresponding Tafel slopes. The polarization.

In respect to the four important criteria for using Levich and Koutecky–Levich equations, typical Koutecky–Levich plots are shown in Fig. 1.16.

As mentioned above the RRDE measurements permit to assess directly the H_2O_2 amount (Fig. 1.17). The fraction of hydrogen peroxide for the Pt-Cr/C is lower than that of Pt/C. The number of electrons involved is close to 4.

The ORR investigations by RRDE permit to assess the main parameters such as the number of electrons involved, the kinetic current density, the exchange current density, the limiting current density, and the Tafel slope in different potential regions. From the bulk materials to the dispersed nanoparticles, the ORR is a key reaction which still needs the development of new electrode materials [191, 192].

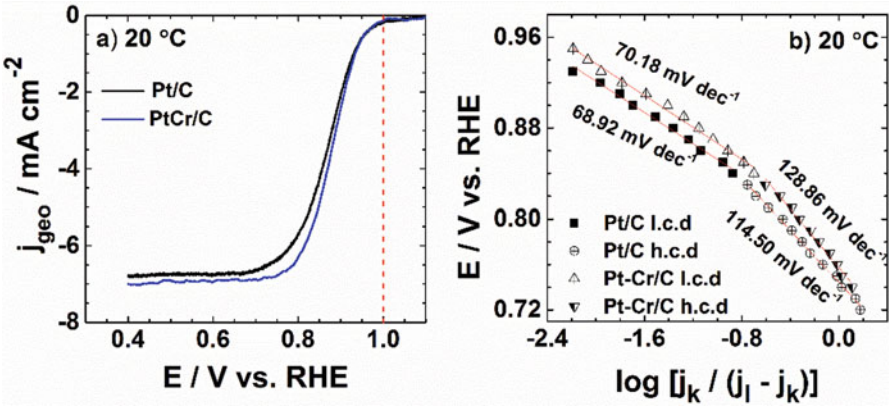

Fig. 1.15 RDE polarization curves of the Pt/C and PtCr/C electrocatalysts in a O_2-saturated 0.1 mol L^{-1} $HClO_4$ solution recorded at 1600 rpm, 5 mV s-1 and (**a**) 20 °C, (**b**) Tafel plots of oxygen reduction reaction on Pt/C and PtCr/C in 0.1 mol L^{-1} $HClO_4$ recorded at 5 mV s^{-1} and 20 °C for low current density (l.c.d) and high current density (h.c.d) region. Reproduced and adapted from Ref. [190] with kind permission of Elsevier©

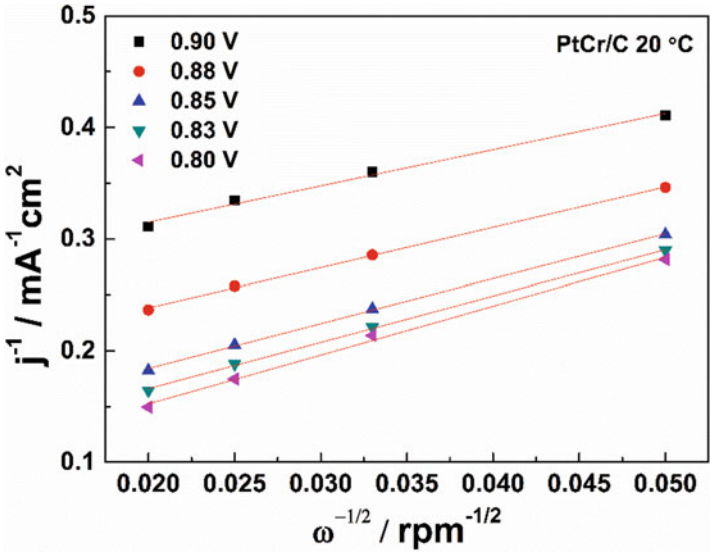

Fig. 1.16 Koutecky–Levich plots (inverse of the current density j versus inverse of the square root of rotation rate ω) of PtCr/C at 20 °C, in 0.1 mol L^{-1} $HClO_4$

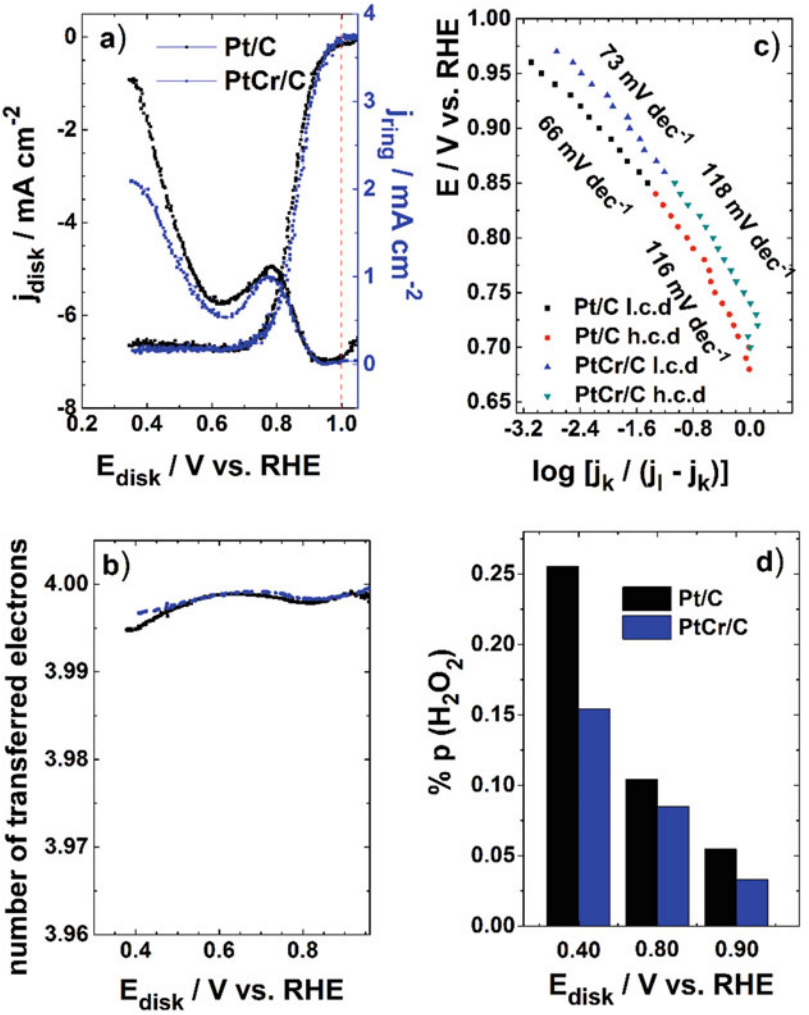

Fig. 1.17 Hydrodynamic voltammograms related to ORR for Pt/C and PtCr/C in a O_2-saturated 0.1 mol L^{-1} $HClO_4$ solution recorded at 5 mV s^{-1} and 1600 rpm. (**a**) Ring electrode and disk electrode current density, (**b**) average number of transferred electrons, (**c**) Tafel plots for low current density (l.c.d) and high current density (h.c.d) regions, and (**d**) fraction of peroxide from the oxygen reduction reaction detected on the ring electrode at 0.90, 0.80, and 0.40 V vs. RHE. From Ref. [190] with kind permission of Elsevier©

1.6 Performance of New Class of Electrode Materials for Proton Exchange Membrane (PEM) Fuel Cells

Both bottom up and top down approaches are used for developing new class of nanomaterials for fuel cell systems in order to considerably increase their performance and durability, but decrease considerably the metal loading. Therefore, oxide materials suggested a support for anode or cathode materials. Figure 1.18 shows three ceria-based anode catalysts prepared with different Pt contents of 0.6, 2, and 4 μg Pt/cm^2 of MEA (the samples denoted 0.6-Pt/Ce, 2-Pt/Ce, and 4-Pt/Ce), and the sputtered reference pure Pt film of 2 μg Pt/cm^2 (2-Pt), all deposited on the nGDL. In a H_2/O_2 fuel cell, the power density of an anode with 2 μg_{Pt} cm^{-2} on ceria is close to that of 2 mg of Pt [193]. The possibility of dividing by 1000 the Pt loading will permit to decrease considerably the cost of the electrodes.

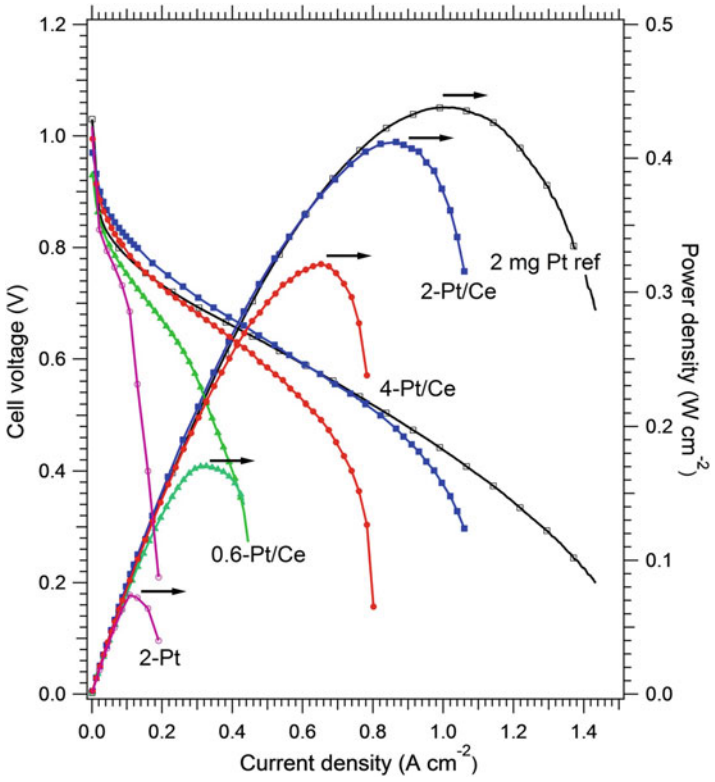

Fig. 1.18 The polarization *J–V* curves (left Y-axis) and the corresponding power density (right Y-axis) measured for the three ceria-based anode catalysts prepared with different Pt contents of 0.6, 2, and 4 μg Pt/cm^2 of MEA (the samples denoted 0.6-Pt/Ce, 2-Pt/Ce, and 4-Pt/Ce), and the sputtered reference pure Pt film of 2 μg Pt/cm^2 (2-Pt), all deposited on the nGDL. For comparison the data obtained on the commercial Pt/GDL catalyst (2 mg Pt ref) are added. From ref. [193] with kind permission of Elsevier©

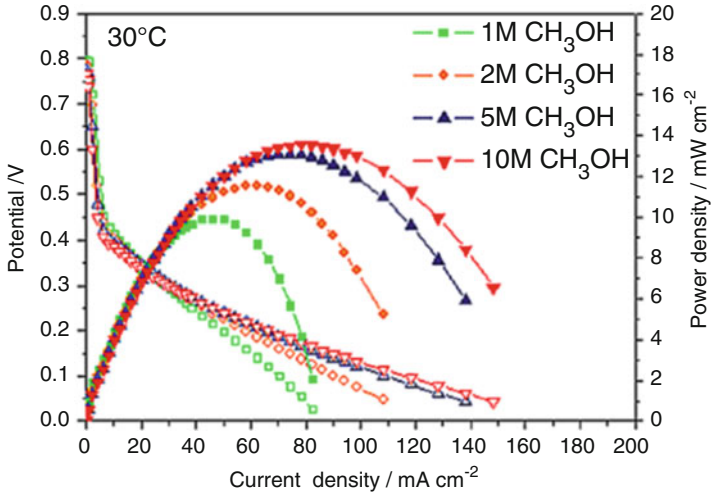

Fig. 1.19 Influence of methanol molarity on DMFC polarization (empty symbols) and power density (filled symbols) curves at 30 °C using the Fe-Nx-C-THT catalyst at the cathode (4.5–-0.2 mg cm^{-2}). Membrane: Nafion® 115. Anode: 1 mg_{PtRu} cm^{-2}. From Ref. [194] with kind permission of copyright Wiley

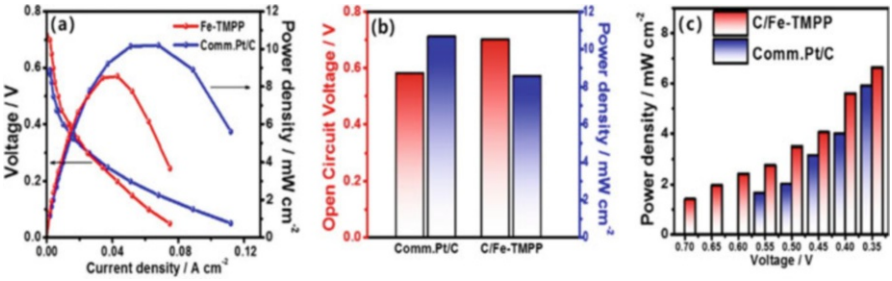

Fig. 1.20 (**a**) Polarization curves of the DEFCs with C/Fe-TMPP and Pt/C as cathode catalysts and PtRu as an anode catalyst supplied with 2 M EtOH and humidified O_2 gas at the anode and cathode, respectively, at 80 °C. (**b**) Comparison of OCVs and maximal power densities of the DEFCs with C/Fe-TMPP and Pt/C. (**c**) Comparison of power densities of the DEFCs with C/Fe-TMPP and Pt/C measured in the potential range of 0.70–0.35 V. From ref. [195] with kind permission of Copyright © 2018 American Chemical Society

One phenomenon which occurs in direct alcohol fuel cells is the crossover of the organic fuel to the cathode. Indeed, the presence of the fuel at the cathode leads to its deactivation. Therefore, cathode with high tolerance to the fuel is required. Figure 1.19 presents the polarization curves of DMFC using Fe-N-C-based catalyst as cathode.

Figure 1.20 shows the performance of a DEFC using a doped carbon nanostructure containing Fe. The DEFC supplied with high concentration of ethanol exhibited

high performance with this cathode. This performance can be attributed to ethanol tolerance in the oxygen reduction reaction [195].

1.7 Conclusion

The last 30 years, progresses have been made in the development of PEMFCs and AEMFCs. In terms of electrode materials, innovation in materials synthesis leads to the fabrication of new class of nanomaterials for anode and cathode of PEMFCs and AEMFCs. For the PEMFCs the metal loadings have been considerably decreased. Various noble metal-free cathodes are suggested for these fuel cells taking into account their tolerance to the liquid fuels such as alcohols and formic acid. For the DMFCs and DEFCs, effective anode nanomaterials are also suggested. AEMFCs are emerging due to the recent development of anion exchange membranes. These membranes offer the possibility to build compact alkaline fuel cells with low-cost materials.

Innovation in materials sciences, nanotechnology, and mechanical engineering is needed to develop powerful PEMFCs and AEMFCs that will be widely available for the world.

References

1. Perry ML, Fuller TF (2002) A historical perspective of fuel cell technology in the 20th century. J Electrochem Soc 149:S59–S67
2. Stone C, Morrison AE (2002) From curiosity to -power to change the world®. Solid State Ionics 152–153:1–13
3. Rodríguez-Varela FJ (2014) Fuel cells, components and systems for space technology applications. Recent Prog Space Technol 4:14–20
4. Gülzow E (2004) Alkaline fuel cells. Fuel Cells 4:251–255
5. https://www.energy.gov/sites/prod/files/2015/11/f27/fcto_fuel_cells_fact_sheet.pdf. Accessed 14 Apr 2018
6. Dekel DR (2018) Review of cell performance in anion exchange membrane fuel cells. J Power Sources 375:158–169
7. Hossen MM, Artyushkova K, Atanassov P, Serov A (2018) Synthesis and characterization of high performing Fe-N-C catalyst for oxygen reduction reaction (ORR) in alkaline exchange membrane fuel cells. J Power Sources 375:214–221
8. Osmieri L, Escudero-Cid R, Monteverde Videla AHA, Ocón P, Specchia S (2018) Application of a non-noble Fe-N-C catalyst for oxygen reduction reaction in an alkaline direct ethanol fuel cell. Renew Energy 115:226–237
9. Ratso S, Kruusenberg I, Käärik M, Kook M, Puust L, Saar R, Leis J, Tammeveski K (2018) Highly efficient transition metal and nitrogen co-doped carbide-derived carbon electrocatalysts for anion exchange membrane fuel cells. J Power Sources 375:233–243
10. Lenarda A, Bellini M, Marchionni A, Miller HA, Montini T, Melchionna M, Vizza F, Prato M, Fornasiero P (2018) Nanostructured carbon supported Pd-ceria as anode catalysts for anion exchange membrane fuel cells fed with polyalcohols. Inorg Chim Acta 470:213–220

11. Basumatary P, Konwar D, Soo Yoon Y (2018) A novel NiCu/ZnO@MWCNT anode employed in urea fuel cell to attain superior performances. Electrochim Acta 261:78–85
12. Qin H, Lin L, Chu W, Jiang W, He Y, Shi Q, Deng Y, Ji Z, Liu J, Tao S (2018) Introducing catalyst in alkaline membrane for improved performance direct borohydride fuel cells. J Power Sources 374:113–120
13. Miller HA, Ruggeri J, Marchionni A, Bellini M, Pagliaro MV, Bartoli C, Pucci A, Passaglia E, Vizza F (2018) Improving the energy efficiency of direct formate fuel cells with a Pd/C-CeO_2 anode catalyst and anion exchange ionomer in the catalyst layer. Energies 11:369–380
14. Muneeb O, Do E, Tran T, Boyd D, Huynh M, Ghosn G, Haan JL (2017) A direct ascorbate fuel cell with an anion exchange membrane. J Power Sources 351:74–78
15. Wagner K, Tiwari P, Swiegers GF, Wallace GG (2018) Alkaline fuel cells with novel gortex-based electrodes are powered remarkably efficiently by methane containing 5% hydrogen. Adv Energy Mater 8:1702285
16. Ziv N, Mustain WE, Dekel DR (2018) Review of ambient CO_2 effect on anion exchange membranes fuel cells. ChemSusChem 11:1–16
17. Piana M, Boccia M, Filpi A, Flammia E, Miller HA, Orsini M, Salusti F, Santiccioli S, Ciardelli F, Pucci A (2010) H_2/air alkaline membrane fuel cell performance and durability, using novel ionomer and non-platinum group metal cathode catalyst. J Power Sources 195:5875–5881
18. Slade RCT, Kizewski JP, Poynton SD, Zeng R, Varcoe JR (2013) Alkaline membrane fuel cells. In: Kreuer KD (ed) Selected entries from the encyclopedia of sustainability science and technology. Springer, New York, pp 9–29
19. Pan ZF, An L, Zhao TS, Tang ZK (2018) Advances and challenges in alkaline anion exchange membrane fuel cells. Prog Energy Combust Sci 66:141–175
20. Sun Z, Lin B, Feng Yan F (2018) Anion-exchange membranes for alkaline fuel-cell applications: the effects of cations. ChemSusChem 11:58–70
21. Omasta TJ, Wang L, Peng X, Lewis CA, Varcoe JR, Mustain WE (2018) Importance of balancing membrane and electrode water in anion exchange membrane fuel cells. J Power Sources 375:205–213
22. Wang L, Brink JJ, Varcoe JR (2017) The first anion-exchange membrane fuel cell to exceed 1 W cm^{-2} at 70 °C with a non-Pt-group (O_2) cathode. Chem Commun 53:11771–11773
23. Gao X, Yu H, Jia J, Hao J, Xie F, Chi J, Qin B, Fu L, Song W, Shao X (2017) High performance anion exchange ionomer for anion exchange membrane fuel cells. RSC Adv 7:19153–19161
24. Gottesfeld S, Dekel DR, Page M, Bae C, Yan Y, Zelenay P, Kim YS (2018) Anion exchange membrane fuel cells: current status and remaining challenges. J Power Sources 375:170–184
25. Strmcnik D, Uchimura M, Wang C, Subbaraman R, Danilovic N, van der Vliet D, Paulikas AP, Stamenkovic VR, Markovic NM (2013) Improving the hydrogen oxidation reaction rate by promotion of hydroxyl adsorption. Nat Chem 5:300–306
26. Miller HA, Lavacchi A, Vizza F, Marelli M, Di Benedetto F, D'Acapito F, Paska Y, Page M, Dekel DR (2016) A Pd/C-CeO_2 anode catalyst for high-performance platinum-free anion exchange membrane fuel cells. Angew Chem Int Ed Engl 55:6004–6007
27. Wang Y, Li L, Hu L, Zhuang L, Lu J, Xu B (2003) A feasibility analysis for alkaline membrane direct methanol fuel cell: thermodynamic disadvantages versus kinetic advantages. Electrochem Commun 5:662–666
28. Hao Yu E, Scott K (2004) Development of direct methanol alkaline fuel cells using anion exchange membranes. J Power Sources 137:248–256
29. Kim JH, Kim HK, Hwang KT, Lee JY (2010) Performance of air-breathing direct methanol fuel cell with anion-exchange membrane. Int J Hydrog Energy 35:768–773
30. Matsuoka K, Iriyama Y, Abe T, Matsuoka M, Ogumi Z (2005) Alkaline direct alcohol fuel cells using an anion exchange membrane. J Power Sources 150:27–31
31. Bambagioni V, Bianchini C, Marchionni A, Filippi J, Vizza F, Teddy J, Serp P, Zhiani M (2009) Pd and Pt–Ru anode electrocatalysts supported on multi-walled carbon nanotubes and

their use in passive and active direct alcohol fuel cells with an anion-exchange membrane (alcohol = methanol, ethanol, glycerol). J Power Sources 190:241–251
32. An L, Zhao TS (2017) Transport phenomena in alkaline direct ethanol fuel cells for sustainable energy production. J Power Sources 341:199–211
33. Wang F, Qiao J, Wu H, Qi J, Li W, Mao Z, Wang Z, Sun W, Rooney D, Sun K (2017) Bioethanol as a new sustainable fuel for anion exchange membrane fuel cells with carbon nanotube supported surface dealloyed PtCo nanocomposite anodes. Chem Eng J 317:623–631
34. Dutta A, Datta J (2012) Outstanding catalyst performance of PdAuNi nanoparticles for the anodic reaction in an alkaline direct ethanol (with anion-exchange membrane) fuel cell. J Phys Chem C 116:25677–22568
35. Fujiwara N, Siroma Z, Yamazaki S, Ioroi T, Senoh H, Yasuda K (2008) Direct ethanol fuel cells using an anion exchange membrane. J Power Sources 185:621–626
36. Li YS, Zhao TS (2016) A passive anion-exchange membrane direct ethanol fuel cell stack and its applications. Int J Hydrog Energy 41:20336–20342
37. Livshits V, Philosoph A, Peled E (2008) Direct ethylene glycol fuel-cell stack—study of oxidation intermediate products. J Power Sources 178:687–691
38. Demirci UB (2009) How green are the chemicals used as liquid fuels in direct liquid-feed fuel cells? Environ Int 35:626–631
39. An L, Zeng L, Zhao TS (2013) An alkaline direct ethylene glycol fuel cell with an alkali-doped polybenzimidazole membrane. Int J Hydrog Energy 38:10602–10606
40. Matsumoto T, Sadakiyo M, Lee Ooi M, Kitano S, Yamamoto T, Matsumura S, Kato K, Takeguchi T, Yamauchi M (2014) CO_2-free power generation on an iron group nanoalloy catalyst via selective oxidation of ethylene glycol to oxalic acid in alkaline media. Sci Rep 4:5620
41. Cremers C, Niedergesäß A, Jung F, Müller D, Tübke J (2011) Development of an alkaline anion exchange membrane direct ethylene glycol fuel cell stack. ECS Trans 41:1987–1996
42. de Souza LL, Neto AO, de O. Forbicini CALG (2017) Direct oxidation of ethylene glycol on PtSn/C for application in alkaline fuel cell. Int J Electrochem Sci 12:11855–11874
43. An L, Zhao TS, Shen SY, Wu QX, Chen R (2010) Performance of a direct ethylene glycol fuel cell with an anion-exchange membrane. Int J Hydrog Energy 35:4329–4335
44. An L, Chen R (2016) Recent progress in alkaline direct ethylene glycol fuel cells for sustainable energy production. J Power Sources 329:484–501
45. Chen Y, Bellini M, Bevilacqua M, Fornasiero P, Lavacchi A, Miller HA, Wang L, Vizza F (2015) Direct alcohol fuel cells: toward the power densities of hydrogen-fed proton exchange membrane fuel cells. ChemSusChem 8:524–533
46. Qi J, Benipal N, Liang C, Li W (2016) PdAg/CNT catalyzed alcohol oxidation reaction for high-performance anion exchange membrane direct alcohol fuel cell (alcohol = methanol, ethanol, ethylene glycol and glycerol). Appl Catal B Environ 199:494–503
47. Ottoni CA, Ramos CED, de Souza RFB, da Silva SG, Spinacé EV, Neto AO (2018) Glycerol and ethanol oxidation in alkaline medium using PtCu/C electrocatalysts. Int J Electrochem Sci 13:1893–1904
48. Ilie A, Simoes M, Baranton S, Coutanceau C, Martemianov S (2011) Influence of operational parameters and of catalytic materials on electrical performance of direct glycerol solid alkaline membrane fuel cells. J Power Sources 196:4965–4971
49. Xin L, Zhang Z, Wang Z, Li W (2012) Simultaneous generation of mesoxalic acid and electricity from glycerol on a gold anode catalyst in anion-exchange membrane fuel cells. ChemCatChem 4:1105–1114
50. Qi J, Xin L, Chadderdon DJ, Qiu Y, Jiang Y, Benipal N, Liang C, Li W (2014) Electrocatalytic selective oxidation of glycerol to tartronate on au/C anode catalysts in anion exchange membrane fuel cells with electricity cogeneration. Appl Catal B Environ 154–155:360–368
51. Qi J, Xin L, Zhang Z, Sun K, He H, Wang F, Chadderdon D, Qiu Y, Liang C, Li W (2013) Surface dealloyed PtCo nanoparticles supported on carbon nanotube: facile synthesis and

promising application for anion exchange membrane direct crude glycerol fuel cell. Green Chem 15:1133–1137
52. Zhiani M, Rostami H, Majidi S, Karami K (2013) Bis (dibenzylidene acetone) palladium (0) catalyst for glycerol oxidation in half cell and in alkaline direct glycerol fuel cell. Int J Hydrog Energy 38:5435–5441
53. Napoleão Geraldes A, da Silva DF, de Andrade e Silva LG, Spinacé EV, Neto AO, dos Santos MC (2015) Binary and ternary palladium based electrocatalysts for alkaline direct glycerol fuel cell. J Power Sources 293:823–830
54. Benipal N, Qi J, Liu Q, Li W (2017) Carbon nanotube supported PdAg nanoparticles for electrocatalytic oxidation of glycerol in anion exchange membrane fuel cells. Appl Catal B Environ 210:121–130
55. Zhang Z, Xin L, Li W (2012) Supported gold nanoparticles as anode catalyst for anion-exchange membrane-direct glycerol fuel cell (AEM-DGFC). Int J Hydrog Energy 37:9393–9401
56. Wang Z, Xin L, Zhao X, Qiu Y, Zhang Z, Baturina OA, Li W (2014) Carbon supported ag nanoparticles with different particle size as cathode catalysts for anion exchange membrane direct glycerol fuel cells. Renew Energy 62:556–562
57. Fashedemi OO, Miller HA, Marchionni A, Vizza F, Ozoemena KI (2015) Electro-oxidation of ethylene glycol and glycerol at palladium-decorated FeCo@Fe core–shell nanocatalysts for alkaline direct alcohol fuel cells: functionalized MWCNT supports and impact on product selectivity. J Mater Chem A 3:7145–7156
58. Han X, Chadderdon DJ, Qi J, Xin L, Li W, Zhou W (2014) Numerical analysis of anion-exchange membrane direct glycerol fuel cells under steady state and dynamic operations. Int J Hydrog Energy 39:19767–19779
59. Jamard R, Latour A, Salomon J, Capron P, Martinent-Beaumont A (2008) Study of fuel efficiency in a direct borohydride fuel cell. J Power Sources 176:287–292
60. Wang L, Magliocca E, Cunningham EL, Mustain WE, Poynton SD, Escudero-Cid R, Nasef MM, Ponce-González J, Bance-Souahli R, Slade RCT, Whelligan DK, Varcoe JR (2017) An optimised synthesis of high performance radiation-grafted anion-exchange membranes. Green Chem 19:831–843
61. Wang Y, Wang G, Li G, Huang B, Pan J, Liu Q, Han J, Xiao L, Lu J, Zhuang L (2015) Pt–Ru catalyzed hydrogen oxidation in alkaline media: oxophilic effect or electronic effect? Energy Environ Sci 8:177–181
62. Alesker M, Page M, Shviro M, Paska Y, Gershinsky G, Dekel DR, Zitoun D (2016) Palladium/nickel bifunctional electrocatalyst for hydrogen oxidation reaction in alkaline membrane fuel cell. J Power Sources 304:332–339
63. Mun Y, Kim MJ, Park SA, Lee E, Ye Y, Lee S, Kim YT, Kim S, Kim OH, Cho YH, Sung YE, Lee J (2018) Soft-template synthesis of mesoporous non-precious metal catalyst with Fe-Nx/C active sites for oxygen reduction reaction in fuel cells. Appl Catal B Environ 222:191–199
64. Hu Q, Li G, Pan J, Tan L, Lu J, Zhuang L (2013) Alkaline polymer electrolyte fuel cell with Ni-based anode and co-based cathode. Int J Hydrog Energy 38:16264–16268
65. Fang Y, Wang Y, Wang F, Shu C, Zhu J, Wu W (2018) Fe–Mn bimetallic oxides-catalyzed oxygen reduction reaction in alkaline direct methanol fuel cells. RSC Adv 8:8678–8687
66. Yang CC (2012) Alkaline direct methanol fuel cell based on a novel anion-exchange composite polymer membrane. J Appl Electrochem 42:305–317
67. Yang CC, Chiu SJ, Lin CT (2008) Electrochemical performance of an air-breathing direct methanol fuel cell using poly(vinyl alcohol)/hydroxyapatite composite polymer membrane. J Power Sources 177:40–49
68. Shu C, Song B, Wei X, Liu Y, Tan Q, Chong S, Chen YZ, Yang XD, Yang WH, Liu Y (2018) Mesoporous 3D nitrogen-doped yolk-shelled carbon spheres for direct methanol fuel cells with polymer fiber membranes. Carbon 129:613–620

69. Ge X, Sumboja A, Wuu D, An T, Li B, Thomas Goh FW, Andy Hor TS, Zong Y, Liu Z (2015) Oxygen reduction in alkaline media: from mechanisms to recent advances of catalysts. ACS Catal 5:4643–4667
70. Mokrini A, Raymond N, Theberge K, Robitaille L, Del Rio C, Ojeda MC, Garcia Escribano P, Acosta JL (2010) Properties of melt-extruded vs. solution-cast proton exchange membranes based on PFSA nanocomposites. ECS Trans 33:855–865
71. Allen FI, Comolli LR, Kusoglu A, Modestino MA, Minor AM, Weber AZ (2015) Morphology of hydrated as-cast nafion revealed through cryo electron tomography. ACS Macro Lett 4:1–5 (https://pubs.acs.org/doi/full/10.1021/mz500606h, further permissions should be directed to the ACS)
72. Kusoglu A, Weber AZ (2017) New insights into perfluorinated sulfonic-acid ionomers. Chem Rev 117:987–1104 (https://pubs.acs.org/doi/full/10.1021/acs.chemrev.6b00159, further permissions should be directed to the ACS)
73. Li J, Pan M, Tang H (2014) Understanding short-side-chain perfluorinated sulfonic acid and its application for high temperature polymer electrolyte membrane fuel cells. RSC Adv 4:3944–3965
74. Paddison SJ, Elliott JA (2006) The effects of backbone conformation on hydration and proton transfer in the short-side-chain perfluorosulfonic acid membrane. Solid State Ionics 177:2385–2390
75. Elliott JA, Paddison SJ (2007) Modelling of morphology and proton transport in PFSA membranes. Phys Chem Chem Phys 9:2602–2618
76. Tse YLS, Herring AM, Kim K, Voth GA (2013) Molecular dynamics simulations of proton transport in 3M and nafion perfluorosulfonic acid membranes. J Phys Chem C 117:8079–8091
77. Schaberg MS, Abulu JE, Haugen G, Emery MA, O'Conner SJ, Xiong PN, Hamrock S (2010) New multi acid side-chain ionomers for proton exchange membrane fuel cells. ECS Trans 33:627–633
78. Giffin GA, Haugen GM, Hamrock SJ, Di Noto V (2013) Interplay between structure and relaxations in perfluorosulfonic acid proton conducting membranes. J Am Chem Soc 135:822–834
79. Gierke TD, Munn GE, Wilson FC (1981) The morphology in nafion perfluorinated membrane products, as determined by wide-angle and small-angle X-ray studies. J Polym Sci Polym Phys 19:1687–1704
80. Tant MR, Darst KP, Lee KD, Martin CW (1989) Structure and properties of short-side-chain perfluorosulfonate ionomers. ACS Sym Ser 15:370–400
81. Moore RB, Martin CR (1989) Morphology and chemical- properties of the dow perfluorosulfonate ionomers. Macromolecules 22:3594–3599
82. Prater K (1990) The renaissance of the solid polymer fuel cell. J Power Sources 29:239–250
83. Gittleman CS, Coms FD, Lai YH (2012) Membrane durability: physical and chemical degradation. In: Mench MM, Kumbur EC, Veziroglu TN (eds) Polymer electrolyte fuel cell degradation. Elsevier, Oxford, pp 15–80
84. Feldheim DL, Lawson DR, Martin CR (1993) Influence of the sulfonate countercation on the thermal stability of nafion@ perfluorosulfonate membranes. J Polym Sci Polym Phys 31:953–957
85. Page KA, Cable KM, Moore RB (2005) Molecular origins of the thermal transitions and dynamic mechanical relaxations in perfluorosulfonate ionomers. Macromolecules 38:6472–6484
86. Page KA, Landis FA, Phillips AK, Moore RB (2006) SAXS analysis of the thermal relaxation of anisotropic morphologies in oriented nafion membranes. Macromolecules 39:3939–3946
87. Mokrini A (2014) Study of azoles as bifunctional additives for proton exchange membranes melt-processing from LSC and SSC perfluorosulfonic acid ionomers. ECS Trans 64:377–388
88. Mokrini A, Toupin M, Malek K (2016) Techno-economics of a new high throughput process for proton exchange membranes manufacturing. World Electric Vehicle J 8:431–442

89. Mokrini A (2017) Ion exchange membranes having low in-plane swelling. US Patent 9,941,538, 10 Apr 2018
90. Grubb WT (1955) Fuel cell. U.S. Patent 2,913,511, 17 Nov 1959
91. Basura VI, Chuy C, Beattie PD, Holdcroft S (2001) Effect of equivalent weight on electrochemical mass transport properties of oxygen in proton exchange membranes based on sulfonated α,β,β-trifluorostyrene (BAM®) and sulfonated styrene-(ethylene-butylene)-styrene triblock (DAIS-analytical) copolymers. J Electroanal Chem 501:77–88
92. Kraytsberg A, Ein-Eli Y (2014) Review of advanced materials for proton exchange membrane fuel cells. Energ Fuel 28:7303–7330
93. D'Agostino VF, Lee JY, Cook EH (1974) Trifluorostyrene sulfonic acid membranes. US Patent 4,012,303, 15 Mar 1977
94. Ding J, Chuy C, Holdcroft S (2002) Enhanced conductivity in morphologically controlled proton exchange membranes: synthesis of macromonomers by SFRP and their incorporation into graft polymers. Macromolecules 35:1348–1355
95. Ding J, Chuy C, Holdcroft SA (2001) A self-organized network of nanochannels enhances ion conductivity through polymer films. Chem Mater 13:2231–2233
96. Enomoto K, Takahashi S, Rohani R, Maekawa Y (2012) Synthesis of copolymer grafts containing sulfoalkyl and hydrophilic groups in polymer electrolyte membranes. J Membrane Sci 36:415–416
97. Gubler L, Gürsel SA, Scherer GG (2005) Radiation grafted membranes for polymer electrolyte fuel cells. Fuel Cells 5:317–335
98. Chen J, Septiani U, Asano M, Maekawa Y, Kubota H, Yoshida M (2007) Comparative study on the preparation and properties of radiation-grafted polymer electrolyte membranes based on fluoropolymer films. J Appl Polym Sci 103:1966–1972
99. Gubler L (2014) Polymer design strategies for radiation-grafted fuel cell membranes. Adv Energy Mater 4:1300827
100. Guzman-Garcia AG, Pintauro PN (1992) Analysis of radiation-grafted membranes for fuel cell electrolytes. J Appl Electrochem 22:204–214
101. Mokrini A, Huneault H, Gerard P (2006) Partially fluorinated proton exchange membranes based on thermoplastic elastomers compatibilized with methyl methacrylate based block copolymers. J Membrane Sci 283(1–2):74–83
102. Mokrini A, Huneault M (2006) Proton exchange membranes based on compatibilized polymer blends of PVDF and SEBS. J Power Sources 154:51–58
103. Babb DA (2002) Polymers from the thermal (2π+2π) cyclodimerization of fluorinated olefins. In: Hougham GG, Cassidy PE, Johns K, Davidson T (eds) Fluoropolymers. I. Synthesis. Kluwer Academic Publishers, New York, pp 25–50
104. Iacono ST, Budy SM, Jin J, Smith DW Jr (2007) Science and technology of perfluorocyclobutyl aryl ether polymers. J Polym Sci Pol Chem 45:5705–5721
105. Mujkic M, Iacono ST, Neilson AR, Smith DW Jr (2009) Recent optical applications of perfluorocyclobutyl aryl ether polymers. Macromol Symp 283−284:326–335
106. Perpall MW, Smith DW Jr, DesMarteau DD, Creager SE (2006) Alternative trifluorovinyl ether derived fluoropolymer membranes and functionalized carbon composite electrodes for fuel cells. Polym Rev 46:297–313
107. Jiang R, Fuller T, Brawn S, Gittleman C (2013) Perfluorocyclobutane and poly(vinylidene fluoride) blend membranes for fuel cells. Electrochim Acta 110:306–315
108. Gubler L, Nauser T, Coms FD, Lai YH, Gittleman CS (2018) Prospects for durable hydrocarbon-based fuel cell membranes. J Electrochem Soc 165:F3100–F3103
109. Kalaw GJD, Wahome JAN, Zhu Y, Balkus KJ Jr, Musselman IH, Yang DJ, Ferraris JP (2013) Perfluorocyclobutyl (PFCB)-based polymer blends for proton exchange membrane fuel cells (PEMFCs). J Membrane Sci 431:86–95
110. Marestin C, Thiry X, Rojo S, Chauveau E, Mercier R (2017) Synthesis of sulfonate ester and sulfonic acid-containing poly(arylene perfluorocyclobutane)s (PFCB) by direct copolymerization of a sulfonate ester-containing precursor. Polymer 108:179–192

111. Roziere J, Jones DJ (2003) Non-fluorinated polymer materials for proton exchange membranes fuel cells. Annu Rev Mater Res 33:503–555
112. Hickner MA, Ghassemi H, Kim YS, Einsla BR, McGrath JE (2004) Alternative polymer systems for proton exchange membranes (PEMs). Chem Rev 104(10):4587–4612
113. Page KA, Rowe BW (2012) An overview of polymer electrolyte membranes for fuel cell applications. In: Page KA, Soles CL, Runt J (eds) Polymers for energy storage and delivery. ACS Symposium Series, Washington, pp 145–164
114. Shin DW, Guiver MD, Lee YM (2017) Hydrocarbon-based polymer electrolyte membranes: importance of morphology on ion transport and membrane stability. Chem Rev 117:4759–4805
115. Shimizu R, Tsuji J, Sato N, Takano J, Itami S, Kusakabe M, Miyatake K, Iiyama A, Uchida M (2017) Durability and degradation analysis of hydrocarbon ionomer membranes in polymer electrolyte fuel cells accelerated stress evaluation. J Power Sources 367:63–71
116. Varcoe JR, Poynton SD, Slade RCT (2009) Alkaline anion-exchange membranes for low-temperature fuel cell application. In: Vielstich W, Lamm A, Gasteiger HA, Yokokawa H (eds) Handbook of fuel cells: fundamentals, technology and applications. Wiley, London, pp 323–335
117. Yanagi H, Fukuta K (2008) Anion exchange membrane and ionomer for alkaline membrane fuel cells (AMFCs). ECS Trans 16:257–262
118. Marino MG, Kreuer KD (2018) Alkaline stability of quaternary ammonium cations for alkaline fuel cell membranes and ionic liquids. ChemSusChem 8:513–523
119. Varcoe JR, Atanassov P, Dekel DR, Herring AM (2014) Anion-exchange membranes in electrochemical energy systems. Energy Environ Sci 7:3135–3191
120. Schwesinger R, Link R, Wenzl P, Kossek S, Keller M (2006) Extremely base-resistant organic phosphazenium cations. Chem Eur J 12:429–437
121. Noonan KJT, Hugar KM, Kostalik HA IV, Lobkovsky EB, Abruña HD, Coates GW (2012) Phosphonium-functionalized polyethylene: a new class of base-stable alkaline anion exchange membranes. J Am Chem Soc 134:18161–18164
122. Luo YT, Guo JC, Wang CS, Chu D (2012) Fuel cell durability enhancement by crosslinking alkaline anion exchange membrane electrolyte. Electrochem Commun 16:65–68
123. Wang LQ, Brink JJ, Liu Y, Herring AM, Ponce-Gonzalez J, Whelligan DK, Varcoe JR (2017) Non-fluorinated pre-irradiation-grafted (peroxidated) LDPE-based anion-exchange membranes with high performance and stability. Energy Environ Sci 10:2154–2167
124. Holade Y, Sahin N, Servat K, Napporn T, Kokoh K (2015) Recent advances in carbon supported metal nanoparticles preparation for oxygen reduction reaction in low temperature fuel cells. Catalysts 5:310
125. Bard AJ, Faulkner LR (2001) Electrochemical methods: fundamentals and applications, 2nd edn. Wiley, New York
126. Ticianelli EA, Derouin CR, Redondo A, Srinivasan S (1988) Methods to advance technology of proton exchange membrane fuel cells. J Electrochem Soc 135:2209–2214
127. Gasteiger HA, Panels JE, Yan SG (2004) Dependence of PEM fuel cell performance on catalyst loading. J Power Sources 127:162–171
128. Cavarroc M, Ennadjaoui A, Mougenot M, Brault P, Escalier R, Tessier Y, Durand J, Roualdes S, Sauvage T, Coutanceau C (2009) Performance of plasma sputtered fuel cell electrodes with ultra-low Pt loadings. Electrochem Commun 11:859–861
129. Croissant MJ, Napporn T, Léger JM, Lamy C (1998) Electrocatalytic oxidation of hydrogen at platinum-modified polyaniline electrodes. Electrochim Acta 43:2447–2457
130. Wang JX, Springer TE, Adzic RR (2006) Dual-pathway kinetic equation for the hydrogen oxidation reaction on Pt electrodes. J Electrochem Soc 153:A1732–A1740
131. Lamy C, Léger J-M, Srinivasan S (2001) Direct methanol fuel cells: from a twentieth century electrochemist's dream to a twenty-first century emerging technology. Kluwer Academic/ Plenum Publishers, New York

132. Velázquez-Palenzuela A, Centellas F, Garrido JA, Arias C, Rodríguez RM, Brillas E, Cabot P-L (2011) Kinetic analysis of carbon monoxide and methanol oxidation on high performance carbon-supported Pt–Ru electrocatalyst for direct methanol fuel cells. J Power Sources 196:3503–3512
133. Abida B, Chirchi L, Baranton S, Napporn TW, Morais C, Léger J-M, Ghorbel A (2013) Hydrogenotitanates nanotubes supported platinum anode for direct methanol fuel cell. J Power Sources 241:429–439
134. Brummel O, Waidhas F, Faisal F, Fiala R, Vorokhta M, Khalakhan I, Dubau M, Figueroba A, Kovacs G, Aleksandrov HA, Vayssilov GN, Kozlov SM, Neyman KM, Matolin V, Libuda J (2016) Stabilization of small platinum nanoparticles on Pt-CeO2 thin film electrocatalysts during methanol oxidation. J Phys Chem C 120:19723–19736
135. Cao J, Chen H, Zhang X, Zhang Y, Liu X (2018) Graphene-supported platinum/nickel phosphide electrocatalyst with improved activity and stability for methanol oxidation. RSC Adv 8:8228–8232
136. El Sawy EN, Birss VI (2018) Nanoengineered Ir-core@Pt-sheII nanoparticles with controlled Pt shell coverages for direct methanol electro-oxidation. ACS Appl Mater Interfaces 10:3459–3469
137. Jasim AM, Hoff SE, Xing Y (2018) Enhancing methanol electrooxidation activity using double oxide catalyst support of tin oxide clusters on doped titanium dioxides. Electrochim Acta 261:221–226
138. Kazemi R, Kiani A (2012) Deposition of palladium submonolayer on nanoporous gold film and investigation of its performance for the methanol electrooxidation reaction. Int J Hydrog Energy 37:4098–4106
139. Li Y, Gao W, Ci L, Wang C, Ajayan PM (2010) Catalytic performance of Pt nanoparticles on reduced graphene oxide for methanol electro-oxidation. Carbon 48:1124–1130
140. Ostroverkh A, Johanek V, Kus P, Sediva R, Matolin V (2016) Efficient ceria-platinum inverse catalyst for partial oxidation of methanol. Langmuir 32:6297–6309
141. Rednyk A, Johanek V, Khalakhan I, Dubau M, Vorokhta M, Matolin V (2016) Methanol oxidation on sputter-coated platinum oxide catalysts. Int J Hydrog Energy 41:265–275
142. Xie J, Zhang Q, Gu L, Xu S, Wang P, Liu J, Ding Y, Yao YF, Nan C, Zhao M, You Y, Zou Z (2016) Ruthenium–platinum core–shell nanocatalysts with substantially enhanced activity and durability towards methanol oxidation. Nano Energy 21:247–257
143. Watanabe M, Motoo S (1975) Electrocatalysis by ad-atoms: part II. Enhancement of the oxidation of methanol on platinum by ruthenium ad-atoms. J Electroanal Chem Interfacial Electrochem 60:267–273
144. Brueckner TM, Pickup PG (2017) Kinetics and stoichiometry of methanol and ethanol oxidation in multi-anode proton exchange membrane cells. J Electrochem Soc 164:F1172–F1178
145. Yuan W, Cheng Y, Shen PK, Li CM, Jiang SP (2015) Significance of wall number on the carbon nanotube support-promoted electrocatalytic activity of Pt NPs towards methanol/formic acid oxidation reactions in direct alcohol fuel cells. J Mater Chem A 3:1961–1971
146. Napporn WT, Laborde H, Léger JM, Lamy C (1996) Electro-oxidation of C1 molecules at Pt-based catalysts highly dispersed into a polymer matrix: effect of the method of preparation. J Electroanal Chem 404:153–159
147. Beyhan S, Uosaki K, Feliu JM, Herrero E (2013) Electrochemical and in situ FTIR studies of ethanol adsorption and oxidation on gold single crystal electrodes in alkaline. J Electroanal Chem 707:89–94
148. Delpeuch AB, Maillard F, Chatenet M, Soudant P, Cremers C (2016) Ethanol oxidation reaction (EOR) investigation on Pt/C, Rh/C, and Pt-based bi- and tri-metallic electrocatalysts: a DEMS and in situ FTIR study. Appl Catal B Environ 181:672–680
149. Pech-Rodriguez WJ, Gonzalez-Quijano D, Vargas-Gutierrez G, Morais C, Napporn TW, Rodriguez-Varela FJ (2017) Electrochemical and in situ FTIR study of the ethanol oxidation reaction on PtMo/C nanomaterials in alkaline media. Appl Catal B Environ 203:654–662

150. Almeida TS, Palma LM, Morais C, Kokoh KB, De Andrade AR (2013) Effect of adding a third metal to carbon-supported ptsn-based nanocatalysts for direct ethanol fuel cell in acidic medium. J Electrochem Soc 160:F965–F971
151. Beyhan S, Coutanceau C, Léger J-M, Napporn TW, Kadırgan F (2013) Promising anode candidates for direct ethanol fuel cell: carbon supported PtSn-based trimetallic catalysts prepared by Bönnemann method. Int J Hydrog Energy 38:6830–6841
152. Buso-Rogero C, Brimaud S, Solla-Gullon J, Vidal-Iglesias FJ, Herrero E, Behm RJ, Feliu JM (2016) Ethanol oxidation on shape-controlled platinum nanoparticles at different pHs: a combined in situ IR spectroscopy and online mass spectrometry study. J Electroanal Chem 763:116–124
153. Erini N, Krause P, Gliech M, Yang R, Huang Y, Strasser P (2015) Comparative assessment of synthetic strategies toward active platinum–rhodium–tin electrocatalysts for efficient ethanol electro-oxidation. J Power Sources 294:299–304
154. García-Rodríguez S, Somodi F, Borbáth I, Margitfalvi JL, Peña MA, Fierro JLG, Rojas S (2009) Controlled synthesis of Pt-Sn/C fuel cell catalysts with exclusive Sn–Pt interaction: application in CO and ethanol electrooxidation reactions. Appl Catal B Environ 91:83–91
155. Higuchi E, Takase T, Chiku M, Inoue H (2014) Preparation of ternary Pt/Rh/SnO2 anode catalysts for use in direct ethanol fuel cells and their electrocatalytic activity for ethanol oxidation reaction. J Power Sources 263:280–287
156. Ishitobi H, Ino Y, Nakagawa N (2017) Anode catalyst with enhanced ethanol electrooxidation activity by effective interaction between Pt-Sn-SiO2 for a direct ethanol fuel cell. Int J Hydrog Energy 42:26897–26904
157. Mahesh I, Jaithaliya R, Sarkar A (2017) Efficient electrooxidation of ethanol on bi@Pt/C nanoparticles: (i) effect of monolayer bi deposition on specific sites of Pt nanoparticle (ii) calculation of average number of e(−)s without help of chemical analysis. Electrochim Acta 258:933–941
158. Majlan EH, Rohendi D, Daud WRW, Husaini T, Haque MA (2018) Electrode for proton exchange membrane fuel cells: a review. Renew Sust Energ Rev 89:117–134
159. Pierozynski B (2012) On the ethanol electrooxidation reaction on catalytic surfaces of Pt in 0.1 M NaOH. Int J Electrochem Sci 7:4261–4271
160. Pierozynski B (2012) Electrooxidation of ethanol on PtRh and PtRu surfaces studied in 0.5 M H2SO4: relation to the behaviour at polycrystalline Pt. Int J Electrochem Sci 7:4488–4497
161. Pierozynski B (2012) Kinetic aspects of ethanol electrooxidation on catalytic surfaces of Pt in 0.5 M H2SO4. Int J Electrochem Sci 7:3327–3338
162. Purgato FLS, Pronier S, Olivi P, de Andrade AR, Leger JM, Tremiliosi-Filho G, Kokoh KB (2012) Direct ethanol fuel cell: electrochemical performance at 90 degrees C on Pt and PtSn/C electrocatalysts. J Power Sources 198:95–99
163. Rizo R, Sebastián D, Lázaro MJ, Pastor E (2017) On the design of Pt-Sn efficient catalyst for carbon monoxide and ethanol oxidation in acid and alkaline media. Appl Catal B Environ 200:246–254
164. Silva JCM, Parreira LS, De Souza RFB, Calegaro ML, Spinacé EV, Neto AO, Santos MC (2011) PtSn/C alloyed and non-alloyed materials: differences in the ethanol electro-oxidation reaction pathways. Appl Catal B Environ 110:141–147
165. Silva LC, Maia G, Passos RR, de Souza EA, Camara GA, Giz MJ (2013) Analysis of the selectivity of PtRh/C and PtRhSn/C to the formation of CO2 during ethanol electrooxidation. Electrochim Acta 112:612–619
166. Soares LA, Morais C, Napporn TW, Kokoh KB, Olivi P (2016) Beneficial effects of rhodium and tin oxide on carbon supported platinum catalysts for ethanol electrooxidation. J Power Sources 315:47–55
167. Xia XH, Liess HD, Iwasita T (1997) Early stages in the oxidation of ethanol at low index single crystal platinum electrodes. J Electroanal Chem 437:233–240

168. Yang YY, Ren J, Li QX, Zhou ZY, Sun SG, Cai WB (2014) Electrocatalysis of ethanol on a Pd electrode in alkaline media: an in situ attenuated total reflection surface-enhanced infrared absorption spectroscopy study. ACS Catal 4:798–803
169. Zhang Z, Xin L, Sun K, Li W (2011) Pd-Ni electrocatalysts for efficient ethanol oxidation reaction in alkaline electrolyte. Int J Hydrog Energy 36:12686–12697
170. Camara GA, de Lima RB, Iwasita T (2005) The influence of PtRu atomic composition on the yields of ethanol oxidation: a study by in situ FTIR spectroscopy. J Electroanal Chem 585:128–131
171. dos Anjos DM, Hahn F, Leger JM, Kokoh KB, Tremiliosi-Filho G (2008) Ethanol electrooxidation on Pt-Sn and Pt-Sn-W bulk alloys. J Braz Chem Soc 19:795–802
172. Garcia-Rodriguez S, Rojas S, Pena MA, Fierro JLG, Baranton S, Leger JM (2011) An FTIR study of Rh-PtSn/C catalysts for ethanol electrooxidation: effect of surface composition. Appl Catal B Environ 106:520–528
173. Kowal A, Gojkovic SL, Lee KS, Olszewski P, Sung YE (2009) Synthesis, characterization and electrocatalytic activity for ethanol oxidation of carbon supported Pt, Pt-Rh, Pt-SnO2 and Pt-Rh-SnO2 nanoclusters. Electrochem Commun 11:724–727
174. Lamy C, Rousseau S, Belgsir EM, Coutanceau C, Léger JM (2004) Recent progress in the direct ethanol fuel cell: development of new platinum–tin electrocatalysts. Electrochim Acta 49:3901–3908
175. Purgato FLS, Olivi P, Leger JM, de Andrade AR, Tremiliosi-Filho G, Gonzalez ER, Lamy C, Kokoh KB (2009) Activity of platinum-tin catalysts prepared by the Pechini-Adams method for the electrooxidation of ethanol. J Electroanal Chem 628:81–89
176. Purgato FLS, Pronier S, Olivi P, de Andrade AR, Léger JM, Tremiliosi-Filho G, Kokoh KB (2012) Direct ethanol fuel cell: electrochemical performance at 90°C on Pt and PtSn/C electrocatalysts. J Power Sources 198:95–99
177. Ribadeneira E, Hoyos BA (2008) Evaluation of Pt–Ru–Ni and Pt–Sn–Ni catalysts as anodes in direct ethanol fuel cells. J Power Sources 180:238–242
178. Ribeiro J, dos Anjos DM, Leger JM, Hahn F, Olivi P, de Andrade AR, Tremiliosi-Filho G, Kokoh KB (2008) Effect of W on PtSn/C catalysts for ethanol electrooxidation. J Appl Electrochem 38:653–662
179. Sen Gupta S, Datta J (2006) A comparative study on ethanol oxidation behavior at Pt and PtRh electrodeposits. J Electroanal Chem 594:65–72
180. Simoes FC, dos Anjos DM, Vigier F, Leger JM, Hahn F, Coutanceau C, Gonzalez ER, Tremiliosi-Filho G, de Andrade AR, Olivi P, Kokoh KB (2007) Electroactivity of tin modified platinum electrodes for ethanol electrooxidation. J Power Sources 167:1–10
181. Sun S, Halseid MC, Heinen M, Jusys Z, Behm RJ (2009) Ethanol electrooxidation on a carbon-supported Pt catalyst at elevated temperature and pressure: a high-temperature/high-pressure DEMS study. J Power Sources 190:2–13
182. Wang Z-B, Yin G-P, Zhang J, Sun Y-C, Shi P-F (2006) Investigation of ethanol electrooxidation on a Pt-Ru-Ni/C catalyst for a direct ethanol fuel cell. J Power Sources 160:37–43
183. Xu C, Shen P k, Liu Y (2007) Ethanol electrooxidation on Pt/C and Pd/C catalysts promoted with oxide. J Power Sources 164:527–531
184. Damjanovic A, Genshaw MA, Bockris JO, apos M (1966) Distinction between intermediates produced in main and side electrodic reactions. J Chem Phys 45:4057–4059
185. Wroblowa HS, Yen Chi P, Razumney G (1976) Electroreduction of oxygen: a new mechanistic criterion. J Electroanal Chem Interfacial Electrochem 69:195–201
186. Hsueh KL, Chin DT, Srinivasan S (1983) Electrode kinetics of oxygen reduction: a theoretical and experimental analysis of the rotating ring-disc electrode method. J Electroanal Chem Interfacial Electrochem 153:79–95
187. Schmidt TJ, Gasteiger HA, Stäb GD, Urban PM, Kolb DM, Behm RJ (1998) Characterization of high-surface-area electrocatalysts using a rotating disk electrode configuration. J Electrochem Soc 145:2354–2358

188. Coutanceau C, Croissant MJ, Napporn T, Lamy C (2000) Electrocatalytic reduction of dioxygen at platinum particles dispersed in a polyaniline film. Electrochim Acta 46:579–588
189. Lim D-H, Wilcox J (2012) Mechanisms of the oxygen reduction reaction on defective graphene-supported Pt nanoparticles from first-principles. J Phys Chem C 116:3653–3660
190. Sahin NE, Napporn TW, Dubau L, Kadirgan F, Leger JM, Kokoh KB (2017) Temperature-dependence of oxygen reduction activity on Pt/C and PtCr/C electrocatalysts synthesized from microwave-heated diethylene glycol method. Appl Catal B Environ 203:72–84
191. Huang Y, Wagner FT, Zhang JL, Jorne J (2014) Hydrogen adsorption on C-supported Pt and Pt-co shell-core nano-catalysts in proton exchange membrane fuel cells: entropic effects and catalytic activity. J Electrochem Soc 161:F653–F659
192. Asset T, Chattot R, Fontana M, Mercier-Guyon B, Job N, Dubau L, Maillard F (2018) A review on recent developments and prospects for the oxygen reduction reaction on hollow Pt-alloy nanoparticles. ChemPhysChem 19(13):1552–1567
193. Fiala R, Figueroba A, Bruix A, Vaclavu M, Rednyk A, Khalakhan I, Vorokhta M, Lavkova J, Illas F, Potin V, Matolinova I, Neyman KM, Matolin V (2016) High efficiency of Pt2+ – CeO2 novel thin film catalyst as anode for proton exchange membrane fuel cells. Appl Catal B Environ 197:262–270
194. David S, Alexey S, Kateryna A, Jonathan G, Plamen A, Aricò AS, Vincenzo B (2016) High performance and cost-effective direct methanol fuel cells: Fe-N-C methanol-tolerant oxygen reduction reaction catalysts. ChemSusChem 9:1986–1995
195. Ma K-B, Kwak D-H, Han S-B, Park H-S, Kim D-H, Won J-E, Kwon S-H, Kim M-C, Moon S-H, Park K-W (2018) Direct ethanol fuel cells with superior ethanol-tolerant nonprecious metal cathode catalysts for oxygen reduction reaction. ACS Sustain Chem Eng 6:7609–7618